NUREG/CR--4667-Vol.8

TI90 012661

Environmentally Assisted Cracking in Light Water Reactors

Semiannual Report
October 1988–March 1989

Manuscript Completed: March 1990
Date Published: June 1990

Prepared by
T. F. Kassner, J.Y. Park, W. E. Ruther,
W. J. Shack, D. R. Diercks, and W. K. Soppet

Argonne National Laboratory
9700 South Cass Avenue
Argonne, IL 60439

Prepared for
Division of Engineering
Office of Nuclear Regulatory Research
U.S. Nuclear Regulatory Commission
Washington, DC 20555
NRC FIN A2212

Previous Documents in Series

Environmentally Assisted Cracking in Light Water Reactors Annual Report October 1983—September 1984, NUREG/CR-4287, ANL-85-33 (June 1985).

Light-Water-Reactor Safety Materials Engineering Research Programs: Quarterly Progress Report October—December 1984, NUREG/CR-3998 Vol. III, ANL-84-60 Vol. III (October 1985).

Light-Water-Reactor Safety Materials Engineering Research Programs: Quarterly Progress Report January—March 1985, NUREG/CR-4490 Vol. I, ANL-85-75 Vol. I (March 1986).

Environmentally Assisted Cracking in Light Water Reactors Semiannual Report April—September 1985, NUREG/CR-4667 Vol. I, ANL-86-31 (June 1986).

Environmentally Assisted Cracking in Light Water Reactors Semiannual Report October 1985—March 1986, NUREG/CR-4667 Vol. II, ANL-86-37 (September 1987).

Environmentally Assisted Cracking in Light Water Reactors Semiannual Report April—September 1986, NUREG/CR-4667 Vol. III, ANL-87-37 (September 1987).

Environmentally Assisted Cracking in Light Water Reactors Semiannual Report October 1986—March 1987, NUREG/CR-4667 Vol. IV, ANL-87-41 (December 1987).

Environmentally Assisted Cracking in Light Water Reactors Semiannual Report April—September 1987, NUREG/CR-4667 Vol. V, ANL-88-32 (June 1988).

Environmentally Assisted Cracking in Light Water Reactors Semiannual Report October 1987—March 1988, NUREG/CR-4667 Vol. 6, ANL-89/10 (August 1989).

Environmentally Assisted Cracking in Light Water Reactors Semiannual Report April—September 1988, NUREG/CR-4667 Vol. 7, ANL-89/40 (March 1990)

Environmentally Assisted Cracking in Light Water Reactors

by

T. F. Kassner, J. Y. Park, W. E. Ruther,
W. J. Shack, D. R. Diercks, and W. K. Soppet

Abstract

This report summarizes work performed by Argonne National Laboratory on environmentally assisted cracking in light water reactors during the six months from October 1988 to March 1989. The effects of load ratio on stress corrosion cracking (SCC) of Types 316NG, 304, and CF-3M cast stainless steels (SSs) were investigated by fracture-mechanics crack-growth-rate (CGR) tests in high-temperature water. The influence of organic impurities on the SCC of Type 316NG SS was also investigated in long-term CGR tests. Tests to determine the susceptibility of 4-in.-diameter Types 316NG and 304 SS pipe weldments to SCC in simulated BWR environments have been conducted. The influence of carbonate at concentrations between 0.1 and 3300 ppm on the SCC behavior of sensitized Type 304 SS in deoxygenated water (<5 ppb) was determined in constant-extension-rate tensile tests. Fatigue tests were conducted on Type 316NG SS in air and BWR environments to assess the degree of conservatism in the ASME Code Section III fatigue design curves. CGR tests are being conducted to determine susceptibility of A533-Gr B low-alloy ferritic steel to SCC in simulated BWR environments.

Contents

List of Figures

List of Tables

Executive Summary

Fracture-mechanics crack-growth-rate (CGR) tests were performed to study stress corrosion cracking (SCC) of Types 316NG and CF-3M cast stainless steel (SS) in oxygenated water with 100 ppb SO_4^{2-}. In these tests, steady-state crack growth in Type 316NG SS under a high load ratio (0.95) was observed only for stress intensities greater than 22 MPa·m$^{1/2}$. Under the same loading conditions, the CGRs of the fine-grain CF-3M cast SS were higher than those of Type 316NG SS. CGR tests on the latter material in oxygenated water containing either propionic or butyric acid at low concentrations (<100 ppb) indicated that neither of these substances mitigated crack growth in this steel, in contrast to results on sensitized Type 304 SS under analogous conditions. A rationale for the difference in behavior of the two steels has been developed.

Tests were performed on 4-in.-diameter Types 316NG and 304 SS pipe weldments in simulated BWR environments at Battelle Pacific Northwest Laboratory under an ANL subcontract. The tests were conducted under cyclic loading conditions with a trapezoidal waveform with 5-min rise and fall times and a 75-min hold period at maximum loads of 193 and 234 MPa. No failures occurred in Type 304 SS pipe weldments during a test time of ≈8500 h in 288°C water containing 100 ppb SO_4^{2-} and a low dissolved oxygen concentration corresponding to hydrogen-water chemistry. At a dissolved oxygen concentration of ≈200 ppb, representative of normal BWR water chemistry, and with 100 ppb SO_4^{2-} as an impurity, through-wall cracks developed in conventional Type 304 SS welds after ≈640 and 750 cycles. Comparable lives were obtained in pipe tests conducted by General Electric Company. A weld overlay repair of one of these weldments lasted 2,726 cycles. The Type 316NG SS pipe weldments have lasted 10 times as long without failure as the reference Type 304 SS pipe weldments.

Fatigue data have been obtained on Type 316NG SS in air and in simulated boiling water reactor (BWR) water at 288°C for comparison with the ASME Section III design curve and the ASME mean data curve. The results in air agree well with the mean data curve for fairly short lives corresponding to plastic strain ranges greater than 0.5%, but fall below the mean data curve at longer lives. Fatigue life in high-temperature water is about half of that in air at a frequency of 0.5 Hz, and the life decreases at lower frequencies in water.

Organic impurities and their decomposition products (e.g., carbonate) could possibly increase susceptibility to localized corrosion and SCC of BWR reactor coolant piping and pressurized water reactor (PWR) secondary-system heat exchanger tube materials. To assess this possiblity, constant-extension-rate tensile (CERT) tests were performed on sensitized Type 304 SS specimens in deoxygenated (≈5 ppb) water containing 0.1 to 3300 ppm CO_3^{2-} over a $pH_{25°C}$ range of 4.0 to 10.6. Transgranular cracking occurred at a low rate that was independent of the CO_3^{2-} concentration in the water. Thus, no increased susceptibility appears to be associated with these impurities.

SCC tests were conducted on fracture-mechanics specimens of A533-Gr B steel. A conventional specimen and others plated with nickel and with gold were used; the plated specimens were intended to provide insight on the possible changes in crack growth behavior that might occur in clad ferritic materials. Composite specimens of A533-Gr B/Inconel-182/Inconel-600 were also fabricated and are being tested. In the same environment and under the same loading conditions, the plated specimens cracked at a higher rate than did the conventional specimen.

1 Introduction

Intergranular stress corrosion cracking (IGSCC) of austenitic SS piping in BWRs has required research, inspection, and mitigation programs that have cost several billion dollars. Other potential environmental degradation problems such as corrosion fatigue must also be considered to ensure the integrity of the reactor pressure boundary. The objective of this program is to develop an independent capability for the assessment of environmentally assisted degradation in LWR systems.

Research during this reporting period focused on (1) SCC of austenitic SS, (2) fatigue of Type 316NG SS, and (3) SCC of ferritic steels used in reactor piping, pressure vessels, and steam generators.

2 Alternative Materials

Alternative materials for recirculation system piping in BWRs such as Types 316NG, 347, and CF-3M SS are very resistant to sensitization and thus are much less susceptible to IGSCC than the Types 304 and 316 SS that were originally used in many operating reactors. However, their resistance to other modes of degradation, such as transgranular (TGSCC) and corrosion-assisted fatigue, must be evaluated over the range of water chemistries encountered in reactor coolant systems.

In the current reporting period, fracture mechanics tests were performed on Types 316NG and CF-3M cast SS to better understand the effects of load ratio and water chemistry on crack growth and to help extend the data base for crack growth rates in these materials to cover all the loading histories and water conditions that can occur in operation.

2.1 Technical Progress

2.1.1 Fracture-Mechanics Crack Growth Tests (W. E. Ruther, J. Y. Park, T. F. Kassner, and W. K. Soppet)

Influence of Stress Intensity and Load Ratio on CGR of Types 316NG and CF-3M Cast SS

Fracture-mechanics crack-growth-rate (CGR) tests were performed on two 0.7T compact-tension specimens, one of CF-3M cast SS (Specimen CTC24-2) and the other of Type 316NG SS (Heat No. D440104, Specimen 104-2). The ferrite level of the cast material was 5%, as determined by magnetic permeability measurements. The specimens were fatigue-precracked in high-temperature water with ≈200 ppb oxygen and 100 ppb SO_4^{2-} at 289°C under a cyclic load with R = 0.25. Crack growth tests were then performed with a cyclic load with R = 0.95 (sawtooth wave shape, 12-s rise and 1-s fall times). Crack lengths were measured by both DC electric potential and compliance techniques; the measurements by the two techniques were in good agreement. The crack lengths as a function of time for the two specimens are shown in Figs. 1 and 2 for Type 316NG and CF-3M SS, respectively, and the CGR data are given in Table 1. Because the fatigue crack growth rate during precracking was higher in the cast specimen, the initial stress intensity factor (K_{max}) under the R = 0.95 loading was ≈21 MPa·m$^{1/2}$ in the Type 316NG SS specimen and ≈22 MPa·m$^{1/2}$ in the CF3M SS specimen.

Table 1. Steady-State Crack Growth Results for Type 316NG and Cast CF-3M SS Specimens[a] at Several Load Ratios[b] in 289°C Water[c] with ≈200 ppb Dissolved Oxygen and 100 ppb Sulfate

			Electrode Potential				Type 316NG SS		Type 304 SS	
Test No.	Time, h	Cond., $\mu S \cdot cm^{-1}$	304 SS, mV(SHE)	Pt, mV(SHE)	Load Ratio	Freq., Hz	K_{max}[d], $MPa \cdot m^{1/2}$	Growth Rate, $m \cdot s^{-1}$	K_{max}[d], $MPa \cdot m^{1/2}$	Growth Rate, $m \cdot s^{-1}$
1	217 1200	0.9	136	120	0.95	0.08	21.4	$<1.0 \times 10^{-12}$	22.6	1.9×10^{-10}
2	1200 1250	0.9	106	66	0.25	0.1	19.0	2.6×10^{-10}	20.7	3.5×10^{-9}
3	1250 1720	0.9	81	41	0.95	0.08	21.6	9.3×10^{-11}	24.0	2.5×10^{-10}
4	1720 2100	1.1	134	95	1.0	0	21.7	4.4×10^{-11}	24.1	3.2×10^{-11}

[a] Compact tension specimens (0.7TCT) of Type 316NG SS (Heat No. D440104; Specimen No. 104-2) and Cast CF-3M SS (Heat No. F5524; Specimen No. CTC24-2). The Type 316NG SS specimen received the following heat treatment: solution-anneal at 1050°C for 0.5 h plus 650°C for 24 h (EPR = 0 C/cm^2), and the CF-3M specimen received no heat treatment.

[b] Positive sawtooth waveform for all load ratios except 0.25, where a sine waveform was used.

[c] Effluent dissolved-oxygen concentration was ≈200 ppb; feedwater oxygen concentration was approximately a factor of 2 higher to compensate for oxygen depletion by corrosion of the autoclave system.

[d] Stress intensity, K_{max}, values at the end of the time period.

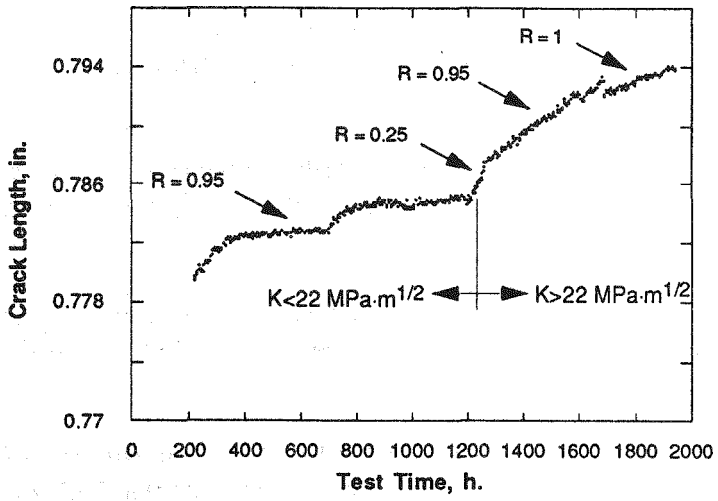

Figure 1. Crack Growth in a Type 316NG SS Specimen under R = 0.25, 0.95, and 1.0 Loading in Water with ≈200 ppb Dissolved Oxygen and 100 ppb Sulfate.

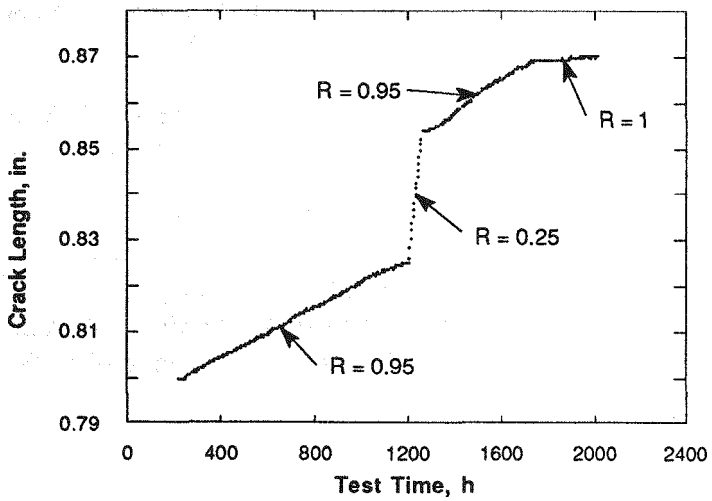

Figure 2. Crack Growth in a CF3M SS Specimen under R = 0.25, 0.95, and 1.0 Loading in Water with ≈200 ppb Dissolved Oxygen and 100 ppb Sulfate.

As shown in Fig. 1, at K_{max} less than ≈22 MPa·m$^{1/2}$, sustained crack growth did not occur in the Type 316NG SS specimen. The transient crack growth shown in the figure at lower K_{max} levels is associated with the loading history changes needed to make the compliance measurements. When a compliance measurement is made, the usual load history must be interrupted by ≈10 cycles of relatively low R loading (0.4). This change in loading history is apparently sufficient to initiate crack growth, which however, cannot be sustained at low K_{max} levels. It is only for K_{max} ≥22 MPa·m$^{1/2}$ that steady-state crack growth was achieved under R = 0.95 loading. Although compliance measurements were still made, no transient behavior was observed, presumably because the steady-state rate under these conditions was relatively high. Thus, a stress intensity of ≈22 MPa·m$^{1/2}$ represents a threshold for growth of SCC in this material under this loading history.

The stress intensity of the cast specimen was always ≥22 MPa·m$^{1/2}$ because of the longer precrack produced by the initial fatigue loading. In this case, steady-state crack growth occurred under the R = 0.95 loading throughout the test. Both materials showed a

decrease in crack growth rate under constant load (R = 1), but the change was much greater in the cast material. The effect is related to environmental crack growth and is not simply due to a change in mechanical fatigue crack growth rate associated with the change in R. Under hydrogen–water chemistry conditions where environmental effects are negligible, no measurable crack growth was observed under R = 0.95 loading.

After the tests in the environment were completed, cracks in the specimens were grown by fatigue in air at room temperature to open the SCC cracks and permit examination of the fracture surfaces. Figure 3 is a scanning electron micrograph of the crack surface of the Type 316NG SS specimen (No. 104–2); it shows a mixture of transgranular and intergranular cracking. The fracture surface of the cast CF–3M SS specimen (No. CTC24–2) shown in Fig. 4 is almost completely transgranular.

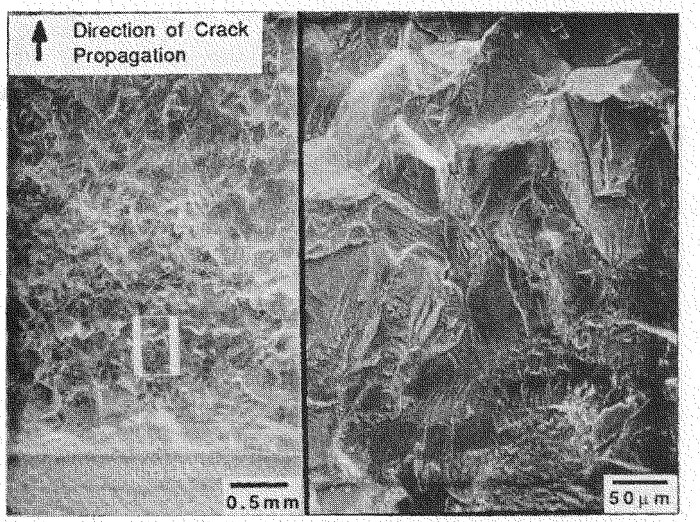

Figure 3. Fracture Surface Morphology of a 0.7TCT Specimen (No. 104–2) of Type 316NG SS after a Crack Growth Experiment at 289°C in the Oxygenated Water with ≈100 ppb Sulfate.

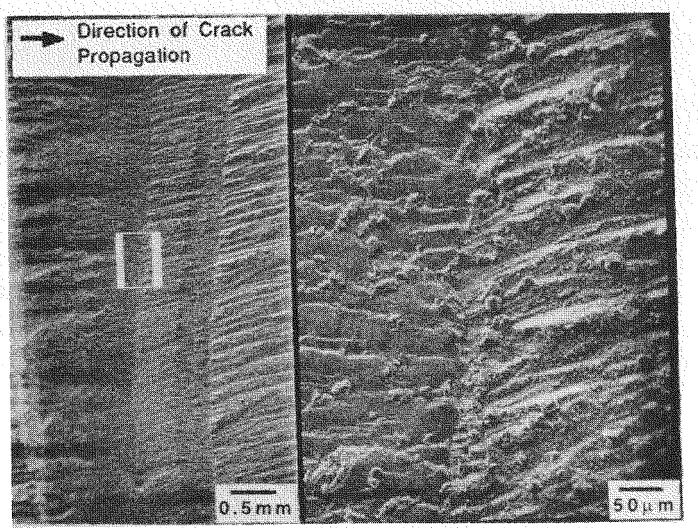

Figure 4. Fracture Surface Morphology of a 0.7TCT Specimen (No. CTC24–2) of Cast CF–3M SS after a Crack Growth Experiment at 289°C in Oxygenated Water with ≈100 ppb Sulfate.

Influence of Organic Acids on CGR of Type 316NG SS

The beneficial effects of several carboxylic acids at low concentrations (<1.0 ppm) on the SCC behavior of sensitized Type 304 SS in oxygenated water in both CERT and fracture-mechanics CGR tests have been reported previously.[1-4] Initial tests indicated however, that these acids were less effective in reducing the CGR of Type 316NG SS. For example, an addition of 1.0 ppm propionic acid halted crack growth in a sensitized Type 304 SS specimen, while the CGR of Type 316NG SS decreased by only a factor of 2.

Table 2 presents results of additional CGR tests on Type 316NG SS in deionized water containing ≈200 ppb dissolved oxygen, in oxygenated water with 0.1 and 1.0 ppm propionic or butyric acid, and in water with 1.0 ppm butyric acid and either 100 ppb SO_4^{2-} or Cl^-. The ECP values of ≈200 mV(SHE) for the Type 304 SS and the platinum electrode and effluent dissolved oxygen values of ≈200 ppb were achieved by oxygen concentrations of 0.4–1.0 ppm in the feedwater. The Type 316NG SS specimen was tested along with a sensitized Type 304 SS specimen. Results for the latter were reported previously.[4]

Crack length as a function of time for 10 test sequences conducted over ≈10,500 h is shown in Figs. 5 and 6. A baseline CGR of 6.7×10^{-11} m·s^{-1} was obtained in deionized water in Test 1 (≈0–1800 h). The addition of 0.1 and 1.0 ppm propionic acid in Tests 2 (≈1800–2500 h) and 3 (≈2500–3600 h) had no effect on the CGR, as can be seen in Table 2 and Fig. 5. However, when propionic acid was no longer added to the feedwater [Test 4 (≈3600–4800 h)], the CGR increased to $\approx 9.0 \times 10^{-11}$ m·s^{-1}, i.e., slightly above the baseline value.

In Test 5 (≈4800–6000 h), 1.0 ppm butyric acid was added to the oxygenated feedwater and the CGR decreased to the baseline value. A decrease in the butyric acid concentration from 1.0 to 0.1 ppm in Test 6 (≈6000–7200 h) caused the CGR to increase by a factor of two. In Test 7 (≈7200–7800 h), the butyric acid concentration in the oxygenated feedwater was increased to 1.0 ppm, and 100 ppb SO_4^{2-} (as H_2SO_4) was also added. As can be seen in Table 2 and Fig. 6, the CGR was not affected. When sulfate was removed from the feedwater in Test 8 (≈7800–8400 h), the CGR decreased significantly to 9×10^{-12} m·s^{-1}. In Test 9 (≈8400–9500 h), 100 ppb Cl^- (as NaCl) was added to the oxygenated feedwater containing 1.0 ppm butyric acid. The CGR of the steel increased by a factor of 40 to $\approx 3.7 \times 10^{-10}$ m·s^{-1}. In the last experiment (No. 10), in which chloride was not added to the feedwater, crack growth continued at the same rate. The results of these tests indicate that the organic acids are not effective in inhibiting crack growth in this material. The influence of ≈100 ppb of either sulfate or chloride on the CGR of the steel was also small in comparison with that observed in sensitized Type 304 SS, where crack growth ceased after removal of these species from the feedwater.[4] Similarly, cracking in Type 316NG SS seems less sensitive to dissolved oxygen levels. In fracture mechanics tests in high-purity water, crack growth in sensitized Type 304 SS specimens almost invariably ceases when the dissolved oxygen concentration is decreased to levels typical of those of a hydrogen-water chemistry, while cracking frequently continues in Type 316NG SS specimens under the same conditions.

Intuitively, it is difficult to rationalize the large differences in the SCC behavior of sensitized Type 304 SS and Type 316NG SS to changes in water chemistry observed in these tests. Other test results suggest that sensitized Type 304 and Type 316NG SS should

Table 2. Crack Growth Results for Type 316NG SS Specimen[a] during Experiments[b] at 289°C in Water Containing ≈200 ppb Dissolved Oxygen,[c] Carboxylic Acids, and Impurity Anions

		Water Chemistry						Electrode Potential		Type 316NG SS	
Test No.	Test Time, h	Organic Acid	Conc., ppm	Impurity Anion[d]	Conc., ppb	pH at 25°C	Cond., $\mu S \cdot cm^{-1}$	304 SS, mV(SHE)	Pt, mV(SHE)	K_{max}[e] $MPa \cdot m^{1/2}$	Growth Rate, $m \cdot s^{-1}$
1	141 1458	–	–	–	–	6.50	0.13	195	200	27.7	0.67×10^{-10}
2	1458 2465	Propionic	0.1	–	–	5.95	0.48	190	190	28.0	0.64×10^{-10}
3	2465 3452	Propionic	1.0	–	–	5.17	3.0	206	220	28.3	0.67×10^{-10}
4	3452 4680	–	–	–	–	6.53	0.12	190	200	28.9	0.90×10^{-10}
5	4680 5836	Butyric	1.0	–	–	5.27	2.5	170	180	29.2	0.64×10^{-10}
6	5836 7182	Butyric	0.1	–	–	6.18	0.38	180	190	30.2	1.20×10^{-10}
7	7182 7566	Butyric	1.0	Sulfate	100	5.18	3.7	190	190	30.5	1.30×10^{-10}
8	7566 8188	Butyric	1.0	–	–	5.23	3.0	190	230	30.6	0.09×10^{-10}
9	8188 9341	Butyric	1.0	Chloride	100	5.21	3.2	200	210	34.5	3.70×10^{-10}
10	9341 10490	Butyric	1.0	–	–	5.16	3.1	175	220	35.8	4.00×10^{-10}

[a] Compact tension specimen (1TCT). AISI 316NG SS (Heat No. P91576; Specimen No. 9P-1) received the following heat treatment: solution-anneal at 1050°C for 0.5 h plus 650°C for 24 h (EPR = 0 $C \cdot cm^{-2}$).

[b] Frequency and load ratio for the positive sawtooth waveform were 8×10^{-2} Hz and 0.95, respectively.

[c] Effluent dissolved-oxygen concentration; feedwater oxygen concentration was 0.4–1.0 ppm.

[d] Sulfate and chloride added as H_2SO_4 and NaCl.

[e] Stress intensity, K_{max}, values at the end of the test condition.

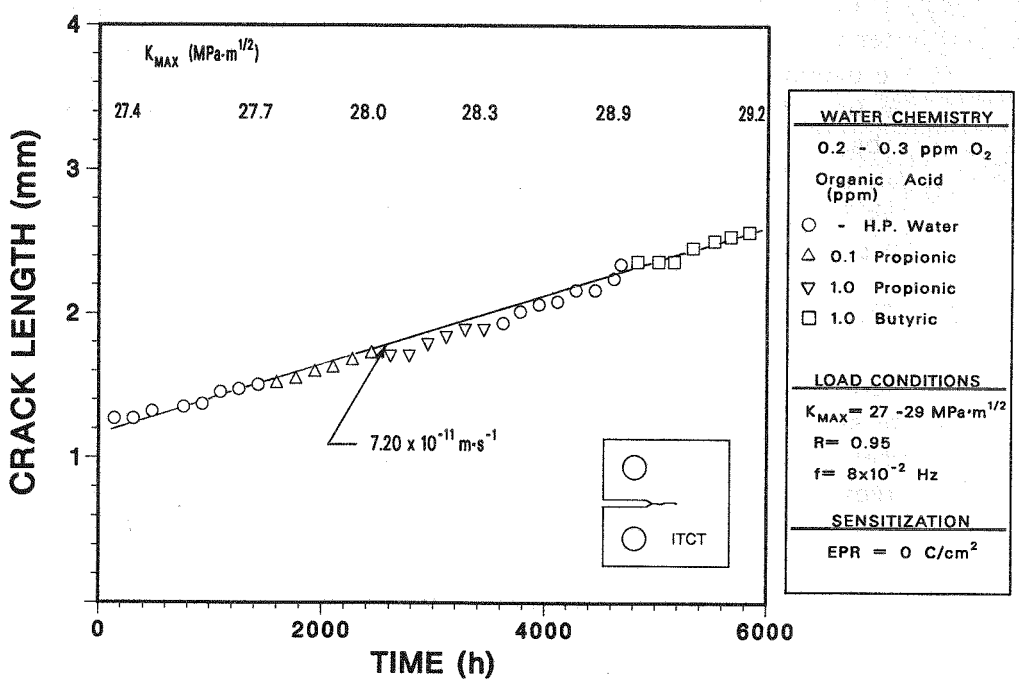

Figure 5. Crack Length versus Time for a 1TCT Specimen of Type 316NG SS in Oxygenated Water (≈200 ppb) without and with 0.1 and 1.0 ppm Propionic Acid at 289°C.

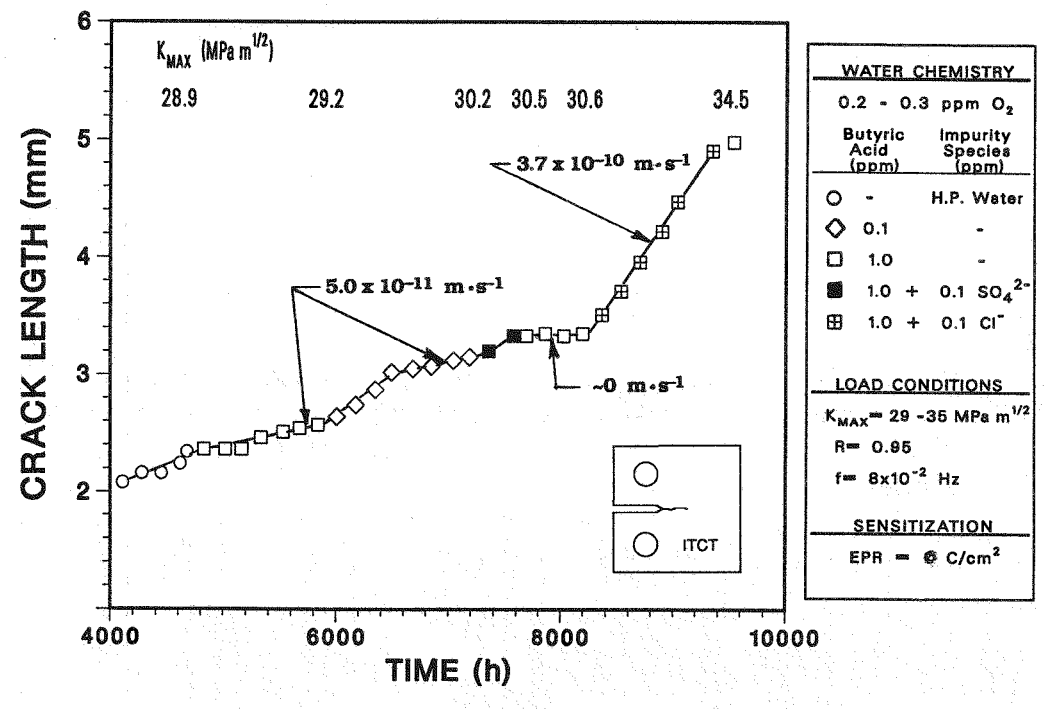

Figure 6. Crack Length versus Time for a Continuation of the Test on a 1TCT Specimen of Type 316NG SS in Oxygenated Water (≈200 ppb) without and with 0.1 ppm Butyric Acid, and 1.0 ppm Butyric Acid without and with 100 ppb of Sulfate or Chloride at 289°C.

behave in a similar manner. The CGRs of these steels usually differ by a factor of less than 2 in oxygenated water under the same loading conditions. In CERT tests at a fixed strain rate in the SCC regime over a range of dissolved oxygen concentration of three orders of magnitude, the CGRs in both steels depend on the concentration of dissolved oxygen to the 1/4–power.[5–7] This observation suggests that the CGRs of the steels are limited by the rate of cathodic reduction of dissolved oxygen. The incremental crack advance per film–rupture event at the crack tip is determined by the stoichiometry and kinetics of the direct $4e^-$ reduction reaction given by the equation

$$O_2 + 2H_2O + 4e^- = 4OH^-. \quad (1)$$

Because the corrosion–product films that form on the two steels in oxygenated water are probably quite similar, the oxygen cathodic reduction processes should also be similar. For example, oxygen adsorption can occur by a bridged configuration where each adsorbed oxygen molecule requires two adjacent vacant sites,[8,9] as depicted by the equation

$$2M + O_2 = \begin{matrix} & O & — & O & \\ & \diagup & & \diagdown & \\ M & & & & M \end{matrix} \quad (O_2 \text{ adsorbed}). \quad (2)$$

In this case, the rate of oxygen reduction, which couples with the rate of anodic dissolution at the crack tip, should be determined primarily by the concentration of active adsorption sites, which presumably does not depend strongly on the differences in the bulk alloy composition of Types 304 and 316NG SS. These arguments seem to suggest that through a site blockage mechanism, organic inhibitors at low concentrations should be equally effective in mitigating SCC of the sensitized and nonsensitized steels, if cathodic reduction of dissolved oxygen is the rate–controlling partial process in both intergranular and transgranular cracking, as postulated. Other factors, which are, however, consistent with the rate–limiting oxygen cathodic reduction partial process, must be considered in order to account for relatively rapid TGSCC of the nonsensitized steels at low dissolved oxygen concentrations and in oxygenated water containing organic substances that can block adsorption sites.

Examination of the intergranular and transgranular crack paths in sensitized and nonsensitized steels gives some insight into the bases for their differences in CGR behavior. In numerous micrographs[10–13] of the type shown in Figs. 7 and 8 for sensitized Type 304 and Type 316NG SS, intergranular cracks are much wider than transgranular cracks. The fracture surfaces and the crack paths shown in Fig. 7 are from two specimens that were tested simultaneously in oxygenated water containing propionic or butyric acid. The test conditions and CGR data for the Type 316NG SS specimen are given in Table 2, and the corresponding information for the sensitized Type 304 SS specimen was presented in Table 13 of the previous report.[4]

The fracture morphologies shown in Figs. 8 and 9 are from specimens in which the sulfate concentration of the oxygenated water was varied from 0 to 100 ppb during a series of tests under high R loading at 289°C. As can be seen in Fig. 9, the SCC crack in the sensitized Type 304 SS specimen (No. 31) branched at the base of the fatigue crack. This cracking pattern is consistent with a slip–dissolution model[14,15] and the expected pattern of shear strains at the tip of the crack. For plane strain deformation in a work–hardening

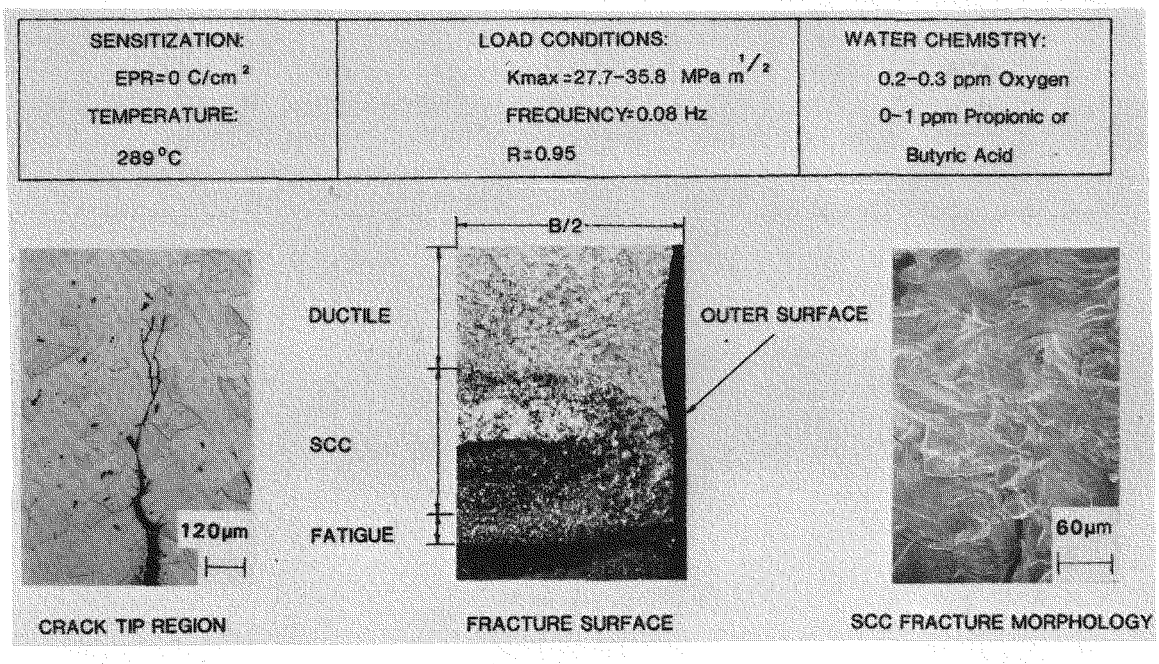

(a)

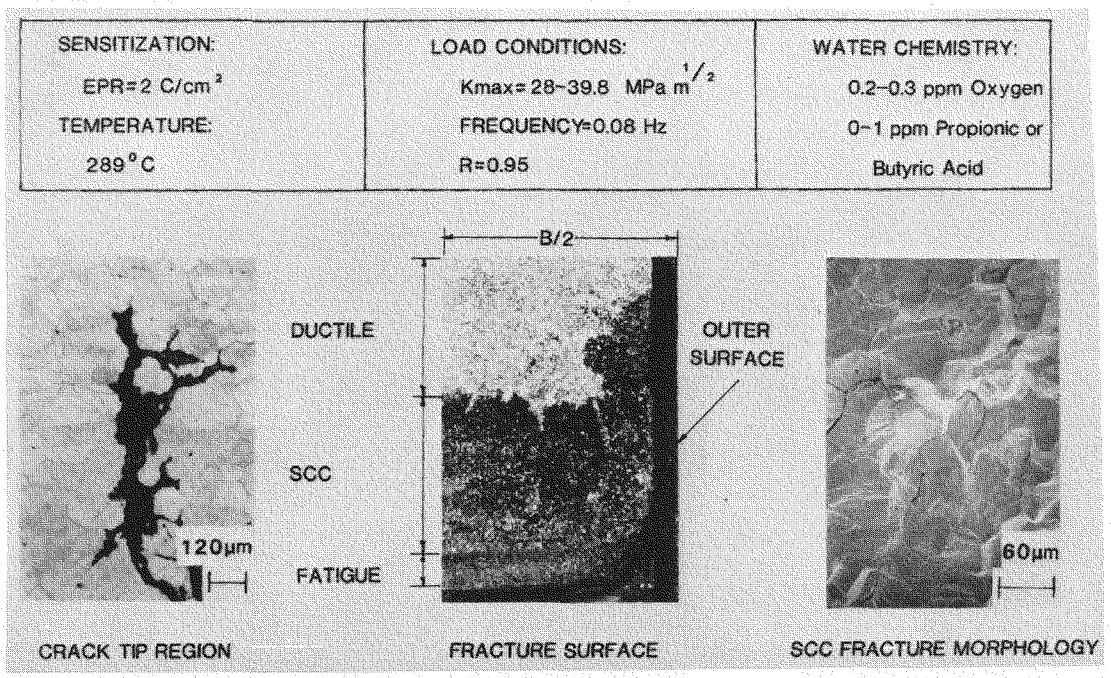

(b)

Figure 7. Fracture Surface and SCC Fracture Morphology of 1TCT Specimens of (a) Type 316NG (Specimen No. P9-1) and (b) Sensitized Type 304 SS (Specimen No. 30) after a Crack Growth Experiment at 289°C with Propionic or Butyric Acid in the Oxygenated Feedwater.

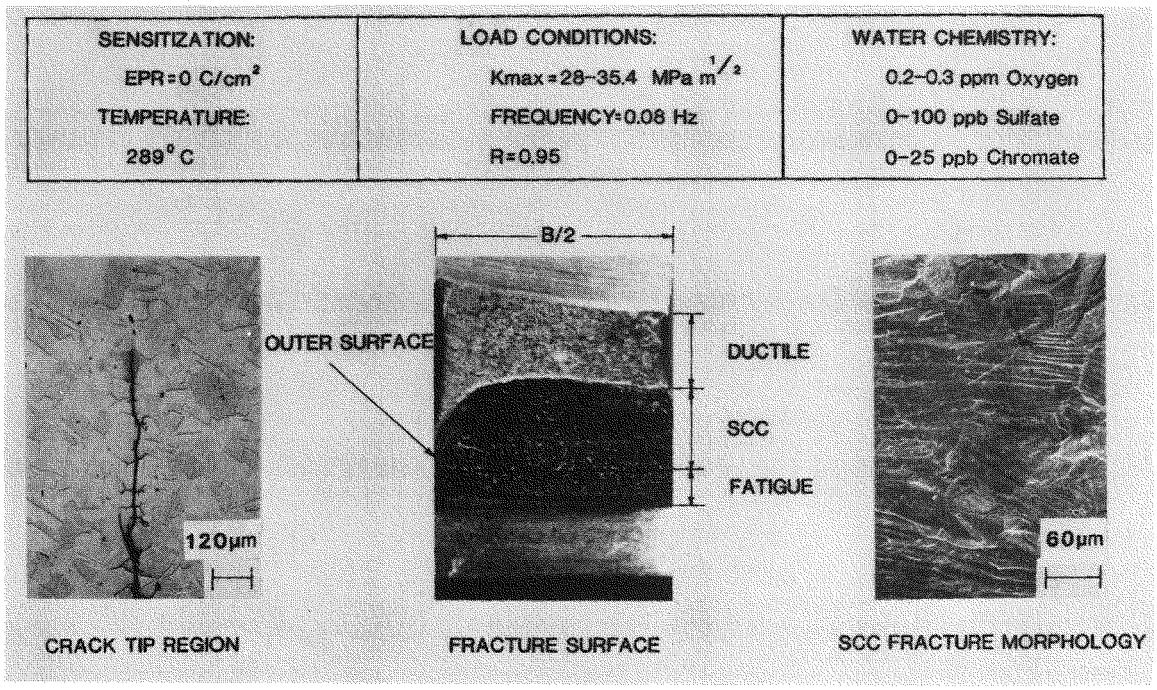

(a)

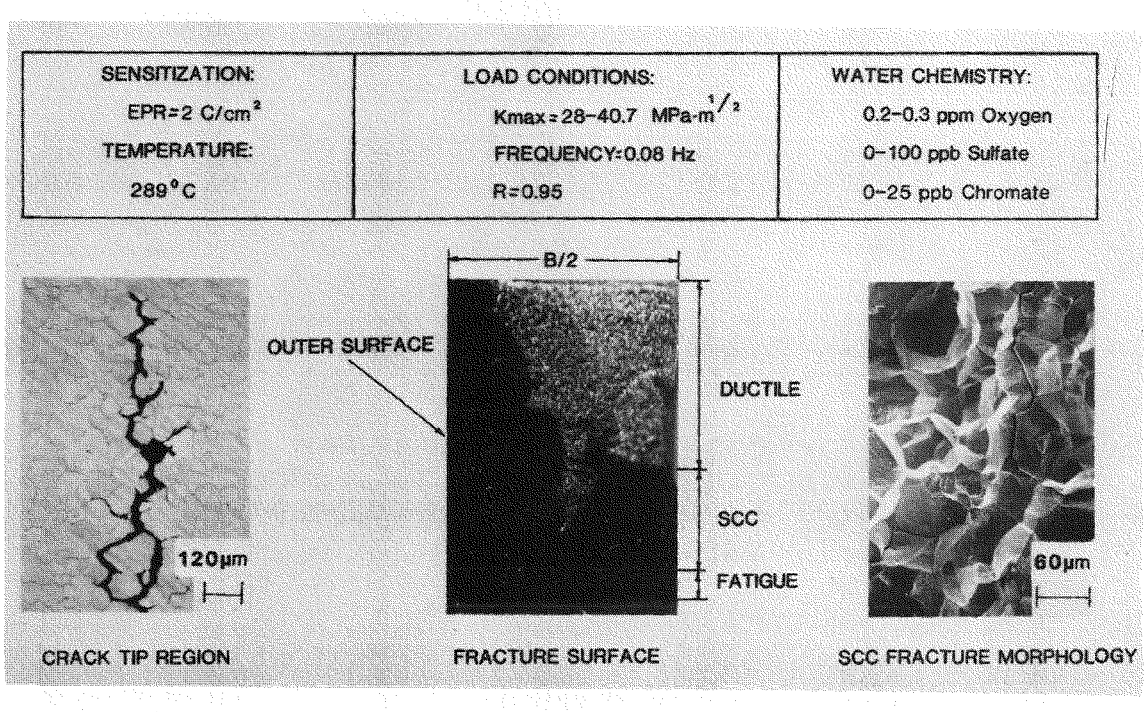

(b)

Figure 8. Fracture Surface and SCC Fracture Morphology of 1TCT Specimens of (a) Type 316NG (Specimen No. P9-2) and (b) Sensitized Type 304 SS (Specimen No. 31) after a Crack Growth Experiment at 289°C with Low Levels of Sulfate or Chromate in the Oxygenated Feedwater.

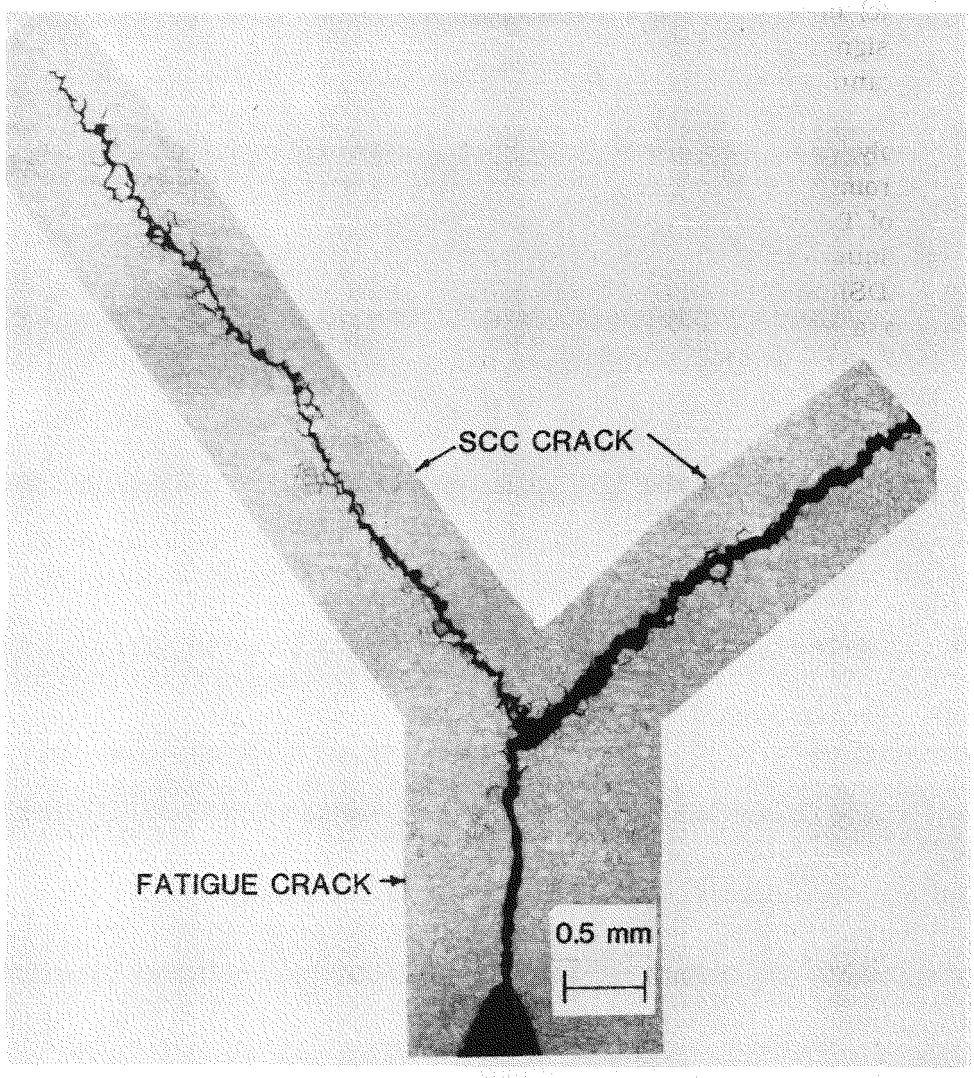

Figure 9. Branched Stress Corrosion Crack at the Base of the Fatigue Crack in a 1TCT Specimen (No. 31) of Sensitized Type 304 SS after a Crack Growth Experiment at 289°C with Low Levels of Sulfate and Chromate in the Oxygenated Feedwater.

material, the directions of maximum shear in front of the crack are at 45° relative to the symmetry line.[16] For crack growth by mechanical loading, even small amounts of work-hardening tend to diffuse the deformation, but in the case of a stress corrosion crack, the plastic strains are very low (only those required to rupture the protective film), and crack growth can remain localized along the 45° slip lines. The CGR data for these specimens appeared in Table 2 of the previous report.[13] Because of the branched nature of the stress corrosion crack, the actual stress intensity values for this specimen are lower than those given in Tables 2 and 3 of the previous report.[13]

Because the tensile properties of Types 304 and 316NG SS are quite similar at 289°C, the crack-opening displacements of cracks with the same length and under the same applied loads would also be similar in the two steels. Consequently, mechanical deformation (nominally elastic) of the noncracked ligament of the compact tension specimens cannot account for the significant differences in the width of the intergranular cracks in sensitized steel and transgranular cracks in solution-annealed Type 304 SS or Type 316NG SS.

Most probably, the differences in the crack widths can be attributed to increased corrosion of the chromium-depleted regions in sensitized steels. Measurements of the degree of sensitization of Types 304 and 316 SS by the electrochemical-potentiodynamic-reactivation (EPR) technique and grain-boundary chromium segregation by energy-dispersive X-ray spectroscopy (EDS) in a scanning-transmission-electron microscope (STEM) have been used to develop a correlation between the EPR value and the width of the chromium depleted zone.[17] The widths of the depleted zones at the grain boundaries (at chromium concentrations of ≈13 and 14 wt.%) increase from ≈2 to 5 nm at an EPR value of ≈2 $C \cdot cm^{-2}$ to ≈10 to 30 nm at an EPR value of ≈20 $C \cdot cm^{-2}$, respectively. These values are only slightly lower than those determined by the STEM-EDS method for CERT specimens from Heat No. 30956 at a chromium concentration of ≈14 wt.%, i.e., ≈10 and 40 nm for EPR values of 2 and 20 $C \cdot cm^{-2}$, respectively.[18] The volume of chromium-depleted material in the grain boundary region exhibits a similar increase with an increase in the degree of sensitization.[17]

In the chromium-depleted region at a sensitized grain boundary, the chromium concentration is ≤13 wt.%, which is significantly lower than in the bulk alloy (≈18-19 wt.%). This difference in composition of the material through which the intergranular and transgranular cracks propagate has important implications for crack growth under cathodic reaction control. The alloy composition at the crack tip and along the crack wall strongly influences the repassivation characteristics, i.e., a high-chromium region repassivates quickly with less metal dissolution/oxidation than does a low-chromium grain-boundary region. Consequently, the electronic charge that is consumed by cathodic reduction of oxygen to sustain anodic dissolution/repassivation of both the crack tip and wall of a sensitized grain boundary in a macrocell corrosion process would be much greater than for the nonsensitized bulk material. Apparently, the cathodic reduction reaction—although diminished by the number of available sites (occupied by organic substances) and/or by low concentrations of dissolved oxygen—is sufficient to sustain anodic dissolution/oxidation of the high-chromium material at the crack tip during TGSCC in a slip-dissolution or oxidation mode of crack advance, because the anodic current associated with the low corrosion rates at the crack walls is very low. In contrast, cathodic reduction cannot balance the anodic current from dissolution/repassivation at both the tip and walls of the intergranular crack, thus limiting crack growth. Crack blunting may also contribute to the cessation of crack growth in the sensitized steel. Several investigators[19-21] have reported on analyses and experimental observations regarding the influence of corrosion of the crack sides and cathodic reduction kinetics at crack surfaces on crack propagation in iron-base alloys.

TGSCC, or a transition from IGSCC to TGSCC, of sensitized Type 304 SS has been considered an "artifact" in CERT tests. However, our argument suggests that this transition in the mode of cracking in low-oxygen water (≤200 ppb) can be attributed to the inability of the cathodic reduction partial process to sustain anodic dissolution/repassivation in the chromium-depleted grain boundary region. A sharp crack, however, can be maintained

Table 3 Influence of Degree of Sensitization of Type 304 SS Specimens[a] on Crack Growth Rate and Fracture Morphology in CERT Tests at 289°C in Water with ≈1.0 and 0.2 ppm Dissolved Oxygen

		Water Chemistry			CERT Parameters		
Test No.	EPR,[b] $C \cdot cm^{-2}$	O_2, ppm	Cond., $\mu S \cdot cm^{-1}$	pH at 25°C	Failure Time, h	CGR,[c] $m \cdot s^{-1}$	Fracture Morphology[d]
71	2	0.87	0.08	6.29	69	12.0×10^{-9}	0.40D, 0.60G_3
90	2	0.99	0.11	6.14	71	9.2×10^{-9}	0.42D, 0.58G_3
86	8	0.95	0.16	6.20	78	9.7×10^{-9}	0.33D, 0.67I
70	20	0.92	0.07	6.41	84	7.0×10^{-9}	0.29D, 0.71I
73	30	0.96	0.12	6.24	85	7.5×10^{-9}	0.55D, 0.45G_3
87	8	0.23	0.09	6.20	100	8.9×10^{-9}	0.42D, 0.58G_3
8	20	0.20	0.20	6.80	119	5.0×10^{-9}	0.32D, 0.68G_1
75	30	0.18	0.10	6.26	143	4.2×10^{-9}	0.81D, 0.19T

[a] Specimens were exposed to the environment for ≈20 h at 289°C before straining at $1 \times 10^{-6}\ s^{-1}$.

[b] Heat treatment conditions that correspond to the degree of sensitization determined by the electrochemical potentiokinetic reactivation (EPR) technique (reactivation charge values, $C \cdot cm^{-2}$) are as follows: 700°C/0.25 h plus 500°C/24 h, EPR = 2 $C \cdot cm^{-2}$; 700°C/0.67 h, EPR = 8 $C \cdot cm^{-2}$; 700°C/12 h, EPR = 20 $C \cdot cm^{-2}$; 700°C/24 h, EPR = 30 $C \cdot cm^{-2}$.

[c] SCC growth rates are based on measurement of depth of the longest crack in an enlarged micrograph of the fracture surface and the time period from the onset of yield to the point of maximum load on the tensile curve.

[d] Ductile (D), transgranular (T), granulated (G), and intergranular (I) characterization of the fracture surface morphologies in terms of the fraction of the cross-sectional area. Characterization of the fracture surface morphologies is in accordance with the definitions in Ref. 22.

Source: Ref. 23.

during repeated film rupture events in the high-chromium material within the grains, which passivates much more rapidly.

CERT data from Type 304 SS specimens with different levels of sensitization (EPR = 2 to 30 $C \cdot cm^{-2}$) in water with ≈0.2 and 1.0 ppm dissolved oxygen concentration (Table 3) indicate that the CGRs decrease as the degree of sensitization increases over the range of 8 to 30 $C \cdot cm^{-2}$.[23] At the lower dissolved oxygen concentration, a transition from intergranular to transgranular cracking occurred as the sensitization increased over this range, whereas at the higher oxygen concentration only IGSCC was observed. At oxygen concentrations of <200 ppb, CGRs did not vary with EPR value; however, a transition from IGSCC to TGSCC occurred as the dissolved oxygen concentration of the deionized water (and the electrochemical potential of the steel) decreased for all levels of sensitization.[23] Thus, the CERT data for the effects of dissolved oxygen and degree of sensitization of Type 304 SS on SCC tend to corroborate the premise that the cathodic reduction partial process can sustain TGSCC of fracture-mechanics specimens of solution-annealed Type 304 or Type 316NG SS in low-oxygen water. This provides a rationale for the relatively high CGRs of the latter steel, in contrast to those of sensitized Type 304 SS, when only a fraction of available sites for oxygen reduction are blocked by carboxylic acids at the 1-ppm level in oxygenated water. In principle, a transition from intergranular to transgranular cracking, rather than no crack growth, could occur in a sensitized fracture-mechanics specimen; however, higher stress

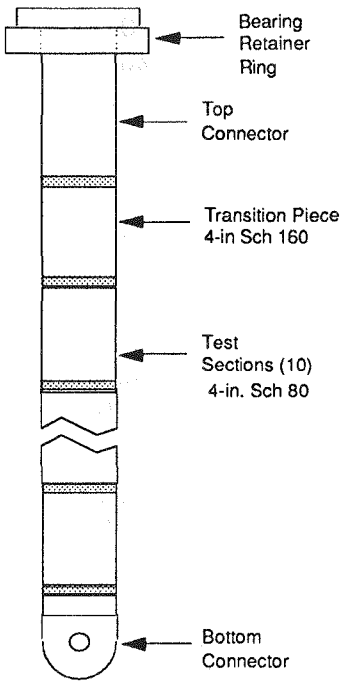

Figure 10. Schematic of Test Specimen for 4-in.-diameter Pipe Tests.

Table 4. Composition of the Pipe Test Materials (wt. %)

Material	Heat No.	Analysis	C	Cr	Ni	Mo	Mn	P	S	Si	N
304 SS	53319	ANL Check	0.06	18.33	8.88	0.14	1.69	0.024	0.013	0.59	0.029
		Vendor	0.06	18.71	8.87	-	1.70	0.028	0.009	0.60	-
316NG	OA2633	ANL Check	0.018	16.64	11.26	2.22	1.71	0.026	0.021	0.28	0.076
		Vendor	0.015	16.49	11.13	2.08	1.71	0.029	0.024	0.29	0.072

intensity values and/or lower R values than those employed in our tests (>40 MPa·m$^{1/2}$, and <0.95, respectively) may be required for this transition to actually be observed.

2.1.2 Tests on Welded Type 316NG and 304 SS Pipe (D. R. Diercks, W. J. Shack, S. G. Pitman,* T. Golding,* and L. Bickford*)

Tests are being performed on 4-in.-diameter Types 316NG and 304 SS welded pipe specimens at Battelle Pacific Northwest Laboratory (PNL) under an ANL subcontract. A schematic of the pipe test assembly is shown in Fig. 10. Ten 100-mm-long segments of the 4-in.-diameter Schedule 80 pipe are joined by circumferential welds to form the test section, and the test section is welded to top and bottom connectors. The compositions of the materials tested are given in Table 4. A Schedule 160 transition piece is placed between the test section and the top connector. Simulated BWR water at 288°C is supplied through an Inconel-600 dip tube that extends down from the top of the test assembly to within ≈50 to 80 mm (2 to 3 in.) of the bottom. The water then flows back out over the

*Battelle Pacific Northwest Laboratory, Richland, WA.

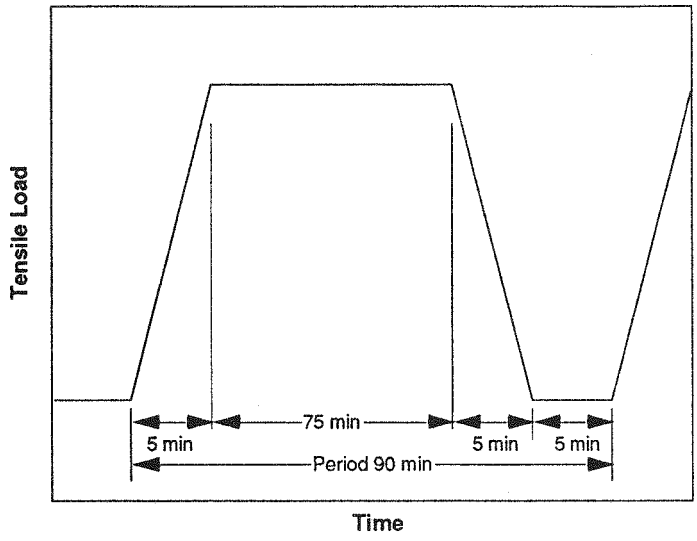

Figure 11. Cyclic Wave Shape Used for 4-in.-diameter Pipe Tests.

inner surface of the test section at a rate of ≈0.3 $L \cdot s^{-1}$ (≈5 gpm). Up to four pipe test specimens can be tested simultaneously.

In addition to the axial and circumferential hydrostatic loads produced by the high-temperature water, cyclic loads are applied to the specimens by a hydraulic loading system. The cyclic wave shape, which is shown schematically in Fig. 11, is similar to that used in pipe tests sponsored by the Electric Power Research Institute at the General Electric Company.[24,25] The nominal water chemistry in the tests is ≈ 200 ppb dissolved oxygen and 100 ppb SO_4^{2-} as H_2SO_4. Initially, these controls were placed on the feedwater, but much of the oxygen was consumed by the test system and the oxygen concentration in the recirculating water was reduced to very low values. In subsequent tests, the dissolved oxygen level of the feedwater was increased to ensure that the effluent dissolved oxygen level was ≈200 ppb.

All of the pipe test specimens have been plagued by fatigue failures in the transition joints at the ends of the test section. These failures are noted in Table 5. The failures have occurred in both the upper and lower weld joints after ≈3,000–7,000 cycles at a maximum stress of 234 MPa and seem to correlate with the number of load cycles independent of the water chemistry. The failures have been examined metallographically by PNL and appear to be due to fatigue. The problem was aggravated by a lack of penetration at the root of the transition welds, which provided starter notches for the fatigue cracks. The most striking characteristic of these failures is the large aspect ratio of the cracks. In all cases, substantial penetration occurred around the complete circumference and the final through-wall opening was typically 270° or larger. This situation is associated with the high degree of pure axial loading achieved in the test stands and the presence of a virtual 360° notch due to poor weld penetration.

The results of the pipe tests, including the fatigue failures encountered in the transition welds, are summarized in Table 5. The initial tests were performed at a relatively low axial stress level of 193 MPa. When no failures occurred, the stress level was increased to 234 MPa, similar to that typical of the GE pipe tests. However, even at the higher stress levels,

Table 5. Summary of Pipe Test Data on Types 316NG and 304 SS

Specimen ID	Material	Heat Number	Accumulated Time at 288°C, h		Accumulated Cycles at 193 MPa Max. Stress	Accumulated Cycles at 234 MPa Max. Stress		Incremental Cycles	Remarks
			Low O_2	High O_2[a]	Low O_2	Low O_2	High O_2[a]		
G	304 SS	53319	8,488	975	3,589	1,319	639	639	Failure of test weld. All test welds in Specimen G overlaid at this time.
			8,488	5,244	3,589	1,319	3,365	2,726	Failure of cracked weld overlay. Failed section replaced with spool piece.
			8,488	6,496	3,589	1,319	4120	755	Failure of repair weld in replacement section.
H	304 SS	53319	8,136	1,326	3,352	1,319	864	864	Transition weld failed; specimen removed from test.
N	316NG	OA2633	2,854	8,502	–	1,319	5,535	5,535	No failures in test welds. Lower transition weld failure. Repaired.
			2,854	10,934	–	1,319	7,118	1,583	Upper transition weld failure. Repaired.
P	316NG	OA2633	2,854	8,177	–	1,319	5,192	5,192	No failures in test welds. Lower transition weld failure. Repaired.
			2,854	12,180	–	1,319	7,734	2,542	Second lower transition weld failure. Repaired.
R	304 SS	–	–	5,800	–	–	3,652	3,652	Improved fabrication technique weld from J.A. Jones. Lower transition weld failure.

[a] Dissolved oxygen concentration of water was ≈200 ppb.

no failures occurred until the dissolved oxygen concentration in the effluent water was increased to the ≈200 ppb level.

Specimens G and H, both fabricated from Type 304 SS, were tested simultaneously. Specimen G ran for 4908 cycles in the low-oxygen environment (3589 cycles at 193 MPa and 1319 cycles at 234 MPa) with no failure. After 639 cycles at 234 MPa in water with ≈200 ppb dissolved oxygen and 100 ppb SO_4^{2-}, one of the test welds failed. All the test welds in this specimen were then overlaid, and testing resumed. After an additional 2,726 cycles, the weld overlay used to repair the initial weld failure cracked, and this segment was removed and replaced by a spool piece. (The failed segment was examined metallographically, and the results are described below.) The welds used to join the replacement spool piece to the remainder of the specimen were not overlaid, and one of these welds failed after an additional 755 cycles; the test was then terminated.

No cracking was observed in Specimens G and H during 8488 h of testing in the low-oxygen environment even with a relatively high impurity level (100 ppb SO_4^{2-}). Since this environment is similar to hydrogen-water chemistry conditions, the result can be interpreted as a verification of the effectiveness of hydrogen-water chemistry in preventing cracking of weld sensitized Type 304 SS. If only the cycles at the 200 ppb oxygen level are considered, the failures after 639 and 755 cycles in the conventional Type 304 SS reference welds of Specimen G are consistent with results of the EPRI/GE pipe tests.[25]

Specimen H ran for 4671 cycles in the low-oxygen environment with no failures, but failed at a transition weld after an additional 864 cycles at 234 MPa in water containing ≈200 ppb oxygen and 100 ppb SO_4^{2-}. At this point, the specimen was removed from testing.

Testing of Type 316NG SS Specimens N and P began while the above tests were in progress. These specimens accumulated 1319 cycles at 234 MPa in low-oxygen water with no failures. Both specimens failed at the lower transition weld after additional cycling (5535 cycles for Specimen N and 5192 cycles for Specimen P) at 234 MPa in water with ≈200 ppb oxygen and 100 ppb SO_4^{2-}. The failed welds of both specimens were repaired and the tests were resumed. Specimen N then failed at the upper transition weld after an additional 1583 cycles, and Specimen P failed again at the lower transition weld after 2542 cycles. These failures are being repaired, and testing will be continued. At present, the test welds in the Type 316NG SS (Specimens N and P) have accumulated 10 times as many cycles without failure as those that produced failure in the reference welds in the Type 304 SS Specimen G.

Specimen R was fabricated from Type 304 SS by the J. A. Jones Applied Research Center in Charlotte, NC, using a variety of machining and/or electrochemical procedures for the final surface preparation of each of the test welds.* However, all welds were made with an improved low-heat-input weld procedure.** This specimen did fail at the lower transition weld after 3652 cycles at 234 MPa in the impurity environment containing ≈200 ppb

*Private communication from D. Grandy, J. A. Jones Applied Research Center, to W. J. Shack, ANL, October 1989.

**Private communication from S. Findlan, J. A. Jones Applied Research Center, to W. J. Shack, ANL, January 1990.

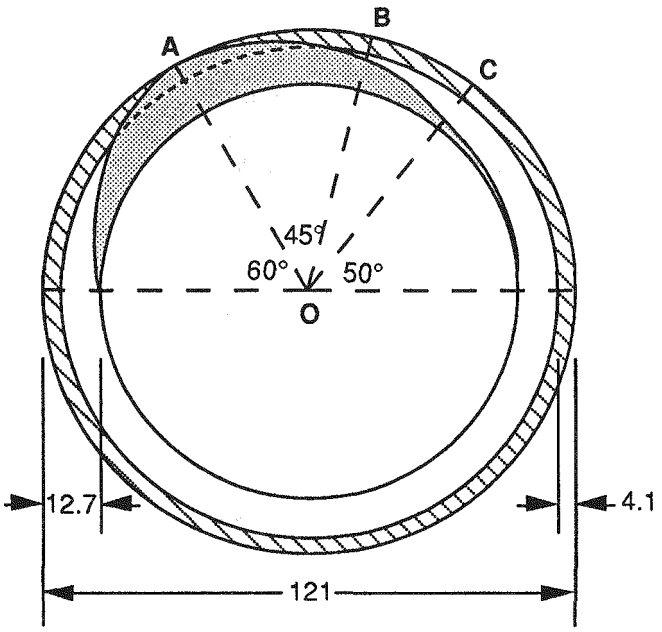

Figure 12. Schematic Representation of Circumferential Section through Failed Pipe Segment from Specimen G. The weld cladding at the OD is shown as the cross-hatched region, and shaded area shows the approximate extent of crack penetration at the time of failure. All dimensions are in mm.

oxygen, but no failures have occurred in the test welds. The lives of the test welds are greater by about a factor of 5 than those of the Type 304 SS Specimen G tested in the same environment. This improvement may be attributable to the improved weld procedure.

The failed test weld in Specimen G was examined to determine the nature and extent of cracking. Dye penetrant examination revealed that while the extent of the crack on the outer diameter (OD) of the failed pipe section was very limited, it extended approximately 180° circumferentially around the inner diameter (ID) surface. On the inner surface, the crack was parallel to and ≈3 to 5 mm from the center line of the circumferential weld and initiated in the weld heat-affected zone.

Figure 12 shows a circumferential section through the failed pipe segment. The weld cladding on the OD is shown as the cross-hatched region, and the shaded area shows the approximate extent of crack penetration at failure. The crack is estimated to have encompassed approximately 20% of the cross section of the pipe. Detailed metallography was performed on the sections OA and OB indicated by the radial dashed lines in Fig. 10.

In section OA, the crack extended completely through the pipe wall, including the weld clad. When viewed in cross-section, the crack was relatively straight and nonbranched. However, some intergranular secondary cracking, suggestive of corrosion-assisted cracking, was observed in the crack near the ID of the pipe (Fig. 13). Near the OD in the weld cladding, no significant secondary cracking was seen.

In section OB, the crack did not reach the weld clad. However, because the original circumferential pipe weld widened with increasing depth into the pipe from the ID surface, the crack penetrated into the weld metal (Fig. 14). Again, the crack was relatively straight

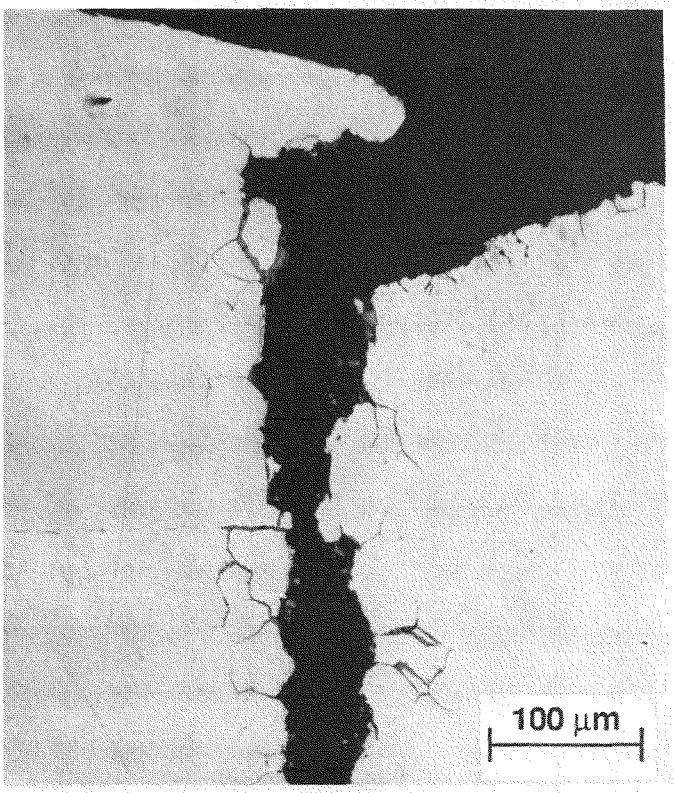

Figure 13. Portion of Metallographic Section OA (Fig. 12) Showing Intergranular Secondary Cracking near the ID Surface.

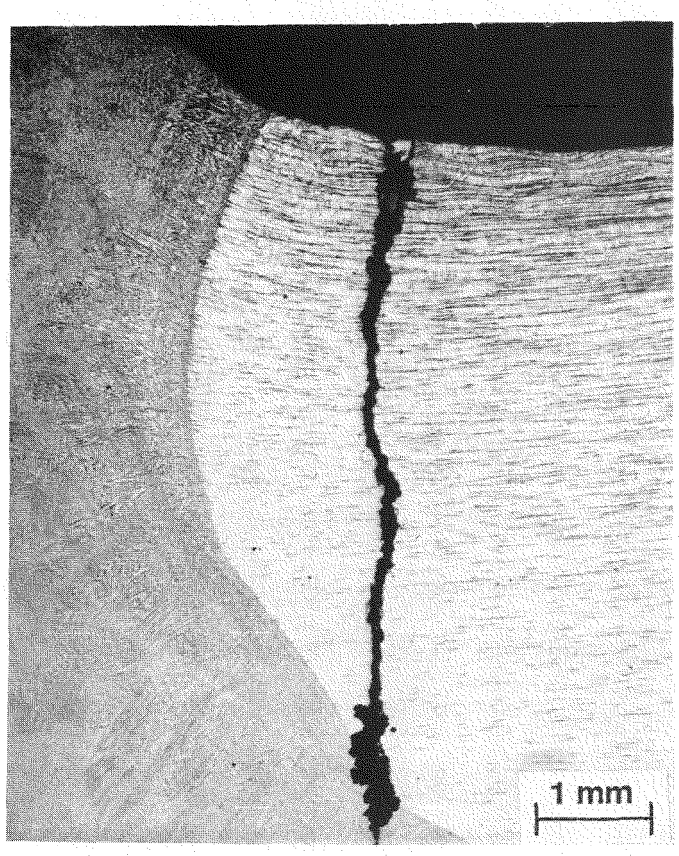

Figure 14. Portion of Metallographic Section OB (Fig. 12) Showing Crack Extending from ID Surface into Test Weld.

Figure 15. SEM Fractograph on Specimen from Section OA (Fig. 12) Showing Presence of Fatigue Striations (Center of Photograph) on Fracture Surface.

and nonbranched, and some intergranular secondary cracking was observed near the mouth of the crack.

Scanning electron microscopy was performed on the fracture surfaces of specimens from section OA. Intergranular secondary cracking was observed near the crack origin. Apparent fatigue striations were observed at a number of locations on the crack face (Fig. 15). This observation, coupled with the relatively straight and nonbranched nature of the cracks, indicates that fatigue was the predominant failure mode. This is not surprising under the relatively high load levels of the pipe tests. Although a crack may initiate by stress corrosion, fatigue dominates the growth of the crack.

2.1.3 Fatigue of Type 316NG SS (W. J. Shack and W. F. Burke)

Tests to provide additional information on the effects of operating temperature and environment on the fatigue behavior of Type 316NG SS have continued. The data provided by these tests are needed to assess the degree of conservatism inherent in the ASME Code Section III Fatigue Design Curves for this material and may also be needed for decisions on life extension beyond the current 40-year design life.

Type 316NG SS test specimens were fabricated from a segment of 22-in.-diameter pipe manufactured by Sumitomo Metal Industries, Ltd., Japan. Baseline in-air tests were performed with the same specimen design and loading systems used for the tests in the environment. However, the tests in air were performed under strain control. The tests in the

Table 6. Comparison of Fatigue Lives of Type 316NG SS in Air and Simulated BWR Coolant

Test No.	Environment	Strain Range, %	Frequency, Hz	Cycles to Failure
1435	Air[a]	0.25	0.33	314,352
1430	Air[a]	0.30	0.33	168,852
1431	Water[b]	0.30	0.5	116,754
1434	Water[b]	0.30	0.05	40,643
1409	Air[a]	0.5	0.5	53,194
1410	Air[c]	0.5	0.5	51,194
1420	Air[d]	0.5	0.5	54,249
1414	Water[b]	0.5	0.5	26,230
1418	Water[b]	0.5	0.5	25,714
1423	Water[b]	0.5	0.05	17,812
1425	Water[b]	0.5	0.005	13,684
1408	Air[a]	0.75	0.33	21,548
1426	Water[b]	0.75	0.5	12,069
1427	Water[b]	0.75	0.05	6,679
1428	Water[b]	0.75	0.005	5,897

[a] Baseline test in air at 288°C under strain control.
[b] High purity water with 200 ppb dissolved oxygen at 288°C.
[c] Baseline test in air at 288°C under stroke control.
[d] Baseline test in air at ~22°C under stroke control in the autoclave.

autoclave are run in stroke control. The stroke values in the autoclave tests were selected to match those measured in the corresponding strain-control test in air. Benchmark tests were performed to show that the lives obtained under the variable-amplitude stroke control were consistent with those obtained under strain control.[26]

The tests in the simulated BWR environment were performed in high-purity water at 288°C with ≈200 ppb dissolved oxygen in the effluent water. The results of the tests to date are summarized in Table 6. A test in the simulated BWR environment at a strain range of 0.25% and a frequency of 0.05 Hz is in progress. It has now run more than 330,000 cycles and shows no indication of approaching failure. The corresponding test in air ran 314,352 cycles. Based on the previous tests at higher strain ranges and shorter lives, failure would have been expected at ≈125,000 cycles. This appears to indicate that the environment has more effect at higher strain ranges, where fatigue life is dominated by crack growth, than at lower strain ranges, where fatigue life is dominated by initiation. However, additional tests must be performed to ensure that the effect is not simply due to data scatter or is an artifact of the test procedure. The in-air test will be repeated using the exact stroke history of the autoclave test to determine a true baseline value for the test.

3 Influence of Water Chemistry on SCC of Type 304 SS

In this work, the potential effectiveness of proposed actions to solve or mitigate the problem of IGSCC in BWR systems through modifications of water chemistry is being evalu-

ated. The effects of dissolved oxygen (produced by radiolytic decomposition of the water), anion impurities (e.g., oxyacids from decomposition of ion exchange resins during intrusions into the primary system), and several corrosion–product cations on the IGSCC susceptibility and crack growth properties of austenitic stainless steels have been studied. Also investigated have been the potential benefits associated with small additions of hydrogen to the coolant under conditions in which ionic impurities (e.g., oxyanions) were present at low concentrations in the high–temperature water.

The results of this work suggest that the crack growth rate of sensitized steel at strain rates in the regime where SCC occurs is limited by the rate of cathodic reduction of dissolved oxygen, various oxyanion impurity species, and Cu^{2+} or Cu^{+} in the high–temperature water. The incremental crack advance per film rupture event at the crack tip is determined by the stoichiometry and kinetics of the individual cathodic reactions. However, crack growth rates increase with crack–tip strain rate because the frequency of film rupture increases. At very high impurity levels (outside the range of simulated BWR water chemistry), crack growth rates become independent of impurity concentration and are limited solely by strain rate, i.e., frequency of film rupture. This interrelationship between mechanical loading conditions (applied or crack–tip strain rate) and water chemistry (concentration of dissolved oxygen, oxyanions, and Cu^{+}) provides the rationale for SCC remedies based on lower residual and operating stresses and lower impurity levels coupled with hydrogen additions to the water to suppress radiolysis of the coolant.

3.1 Technical Progress

3.1.1 Effect of Carbonate in Water with ≈5 ppb Dissolved Oxygen on SCC (W. E. Ruther, W. K. Soppet, and T. F. Kassner)

Organic impurities and their decomposition products (e.g., CO_3^{2-}, HCO_3^{-}) are a potential concern in BWR water and PWR secondary–system water in terms of increased susceptibility to localized corrosion and SCC of piping and heat–exchanger tube materials. Typical chemicals at power plants include paint products, glycol, hydraulic fluids, lubricants, detergents, chemical cleaners, laundry chemicals, freons, diesel fuel, and ion–exchange resin regeneration chemicals. Potential chemical contaminants[27] and possible pathways[28] for entry of various substances into BWR coolant systems have been evaluated. Some long–lived products that may exist in BWR water due to organic intrusions are carboxylic acids, alcohols, phenolics, aromatic hydrocarbons, hydrogen halides, sulfuric and sulfonic acids, amines, and other substances.[27]

Organic impurities are also a concern in PWR secondary–coolant water systems because organic acids increase cation conductivity, which complicates secondary water monitoring and control. A recent survey of organic acids, total organic carbon, and inorganic anions in the PWR secondary water cycle indicated that organic acids were responsible for a major fraction of the cation conductivity in many plants.[29] Most common were acetic and formic acids; however, lactic, propionic, and butyric acids were also present in some systems. Make–up water was the major source of the organic impurities, some of which were in colloidal, nonionic form.[29] The organic acids can ultimately decompose to form carbonate in reactor coolant circuits.

The effect of carbonate on SCC of sensitized Type 304 SS was investigated by CERTs in water with ≈5 ppb dissolved oxygen. Carbonate was added to the feedwater as either H_2CO_3 by bubbling the deoxygenated feedwater with N_2/CO_2 gas mixtures and maintaining different cover gas pressures over the feedwater or by adding Na_2CO_3 to the water (100% N_2 cover gas). The carbonate concentrations and the range of $pH_{25°C}$ values obtained by the two methods were ≈25 to 3300 with $pH_{25°C}$ = 5.3 to 3.9 and ≈0.1 to 25 ppm with $pH_{25°C}$ = 7.1 to 10.6, respectively. Analogously to our previous results on the effect of dissolved oxygen and various oxyanions on SCC of the steel,[5,30,31] if cathodic reduction of the carbonate ion to formate is the rate-controlling step in the overall SCC process and occurs according to the reaction

$$CO_3^{2-} + H_2O + 2e^- = CO_2^{2-} + 2OH^- \quad (2)$$

the corresponding chemical equilibrium can be written as

$$K_{eq} = (OH^-)^2 (CO_2^{2-}) / (e^-)^2(CO_3^{2-}) \quad (3)$$

and the reciprocal of the electron concentration would depend on the concentration of carbonate as given by the following equation:

$$1/(e^-) = k_1 (CO_3^{2-})^{1/2} / (OH^-) (CO_2^{2-})^{1/2}. \quad (4)$$

Because the CGR is proportional to $1/(e^-)$ for many impurity species that undergo cathodic reduction,[5,30-34] Eqs. (2)–(4) indicate that the CGR should depend on the 1/2-power of the carbonate concentration in low-oxygen water for the electrochemical potential–pH regime corresponding to Eq. (2), if cathodic reduction of the carbonate ion is the rate-controlling step.

The experimental results in Table 7 and Fig. 16 indicate that the CGRs do not exhibit this dependence over the wide range of carbonate concentration, conductivity, and $pH_{25°C}$ of the feedwater examined in the tests. Only TGSCC occurred at an average rate of $(2.8 \pm 1.2) \times 10^{-9}$ m·s^{-1} over this range of conditions. Carbonate is the only oxyanion species that is capable of cathodic reduction (to formate), in which the CGRs during CERT tests in deoxygenated water at 289°C have not exhibited a $1/(e^-)$ dependence on the concentration of the anion raised to a simple power (e.g., 1/2 from Eq. [4]). Apparently, carbonate is either a very stable ion and the reaction in Eq. (2) is not favorable or electron transport through the corrosion product film is minimal under the potential/pH conditions of these experiments, i.e., the electrochemical potential (ECP) values are considerably below the critical potential for IGSCC, as discussed below.

The dependence of ECP of the steel and the platinum electrode on carbonate concentration of the feedwater in the CERTs is shown in Fig. 17. The ECP values for Type 304 SS in acidic solutions (H_2CO_3) increase from ≈–570 to –460 mV(SHE) over the concentration range of ≈25 to 3300 ppm CO_3^{2-}, whereas the ECP of platinum [–500 mV(SHE)] does not vary with carbonate concentration over this range. In basic solutions (Na_2CO_3), the ECP values of both the steel and platinum decrease from ≈–500 to –720 mV(SHE) over the concentration range of ≈0.1 to 25 ppm. The ECP values in Figs. 18 and 19 can be rationalized in terms of their dependence on $pH_{289°C}$ or $pH_{25°C}$, which show similar trends. The ECP

Table 7. Influence of H_2CO_3 and Na_2CO_3 at Low Dissolved-Oxygen Concentration (<5 ppb) on SCC Susceptibility of Sensitized Type 304 SS Specimens[a] in 289°C Water

	Feedwater Chemistry					CERT Parameters						Potential	
Test No.	Cover Gas[b], %	Anion Conc., ppm	Cond. at 25°C, $\mu S \cdot cm^{-1}$	pH at 25°C	pH at 289°C[c]	Failure Time, h	Maximum Stress, MPa	Total Elong., %	Reduction in Area, %	SCC Growth Rate,[d] $m \cdot s^{-1}$	Fracture Morphology[e]	Type 304 SS, mv(SHE)	Pt, mv(SHE)
A161[f]	100% N_2	0.1	0.46	7.10	5.92	122	507	44	47	3.2×10^{-9}	0.88D, 0.12T	-523	-495
A160[f]	100% N_2	5	27.0	10.24	7.45	130	501	47	50	3.0×10^{-9}	0.63D, 0.37T	-681	-666
A159[f]	100% N_2	25	123.0	10.63	8.09	134	511	48	52	3.1×10^{-9}	0.56D, 0.44T	-716	-720
A158	N_2-1% CO_2	24	2.9	5.28	5.56	123	503	44	49	2.3×10^{-9}	0.66D, 0.34T	-579	-496
A156	N_2-4% CO_2	96	5.8	4.97	5.44	123	506	44	40	2.7×10^{-9}	0.73D, 0.27T	-555	-497
A154	N_2-10% CO_2	240	10.5	4.70	5.30	134	522	48	55	1.2×10^{-9}	0.80D, 0.20T	-551	-475
A155	N_2-40% CO_2	960	15.2	4.52	5.05	115	501	41	39	4.0×10^{-9}	0.61D, 0.39T	-545	-507
A153	100% CO_2	2400	46.5	3.97	4.83	122	511	44	43	3.4×10^{-9}	0.65D, 0.35T	-462	-515
A157[g]	100% CO_2	3300	50.0	3.94	4.78	121	501	43	44	2.3×10^{-9}	0.73D, 0.27T	-497	-434

[a] Lightly sensitized (EPR = 2 $C \cdot cm^{-2}$) specimens (Heat No. 30956) were exposed to environments for ≈20 h before being strained at 1×10^{-6} s^{-1}.

[b] Composition of cover gas over feedwater at pressure of 3 psig at 25°C.

[c] Calculated $pH_{289°C}$ on the basis of measured $pH_{25°C}$ values and the dissociation constant for water and the first and second dissociation constants for carbonic acid and sodium carbonate.

[d] SCC growth rates are based on measurement of depth of longest crack in an enlarged micrograph of the fracture surface and of time from onset of yield to point of maximum load on the tensile curve.

[e] Ductile (D), transgranular (T), granulated (G), and intergranular (I), in terms of the fraction of the cross-sectional area. Characterization of the fracture surface morphologies is in accordance with the illustrations and definitions in Ref. 22.

[f] Carbonate added as Na_2CO_3.

[g] Cover gas at overpressure of 9.5 psig at 25°C.

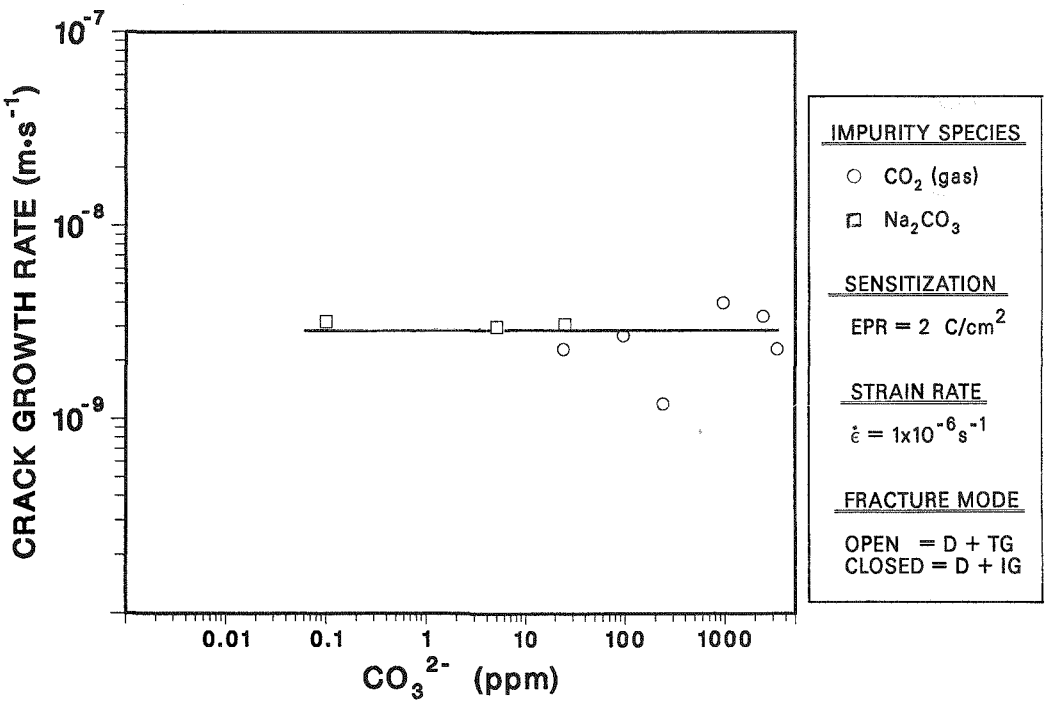

(a)

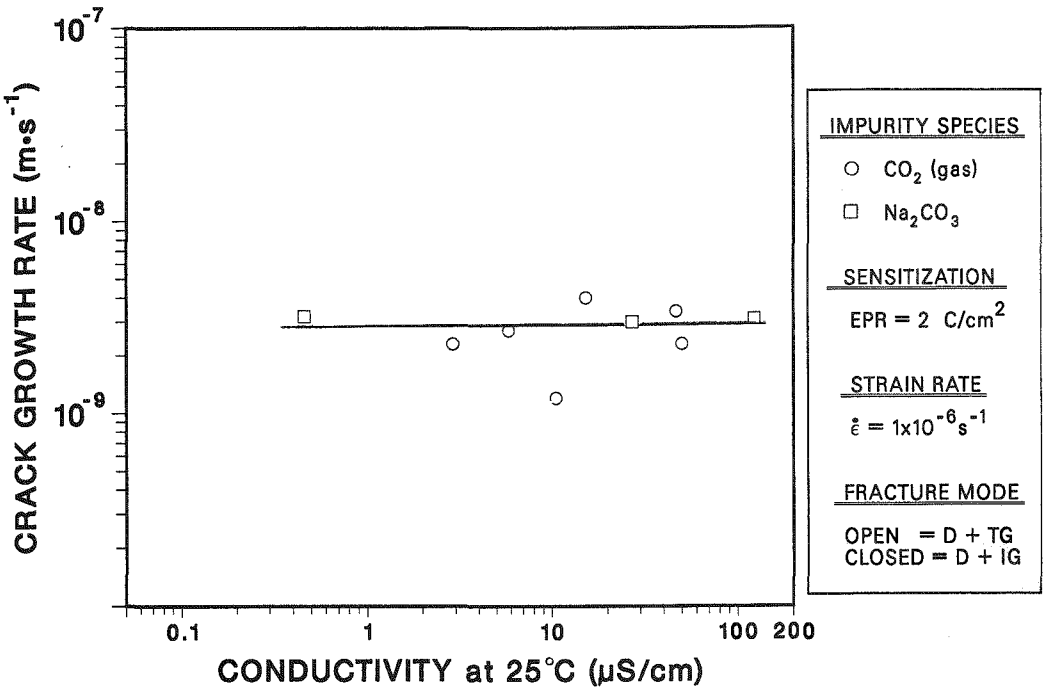

(b)

Figure 16. Dependence of the CGR of Sensitized Type 304 SS CERT Specimens at 289°C on (a) Concentration of Carbonate, (b) Conductivity, and (c) $pH_{25°C}$ of the Low-Oxygen (<5 ppb) Feedwater.

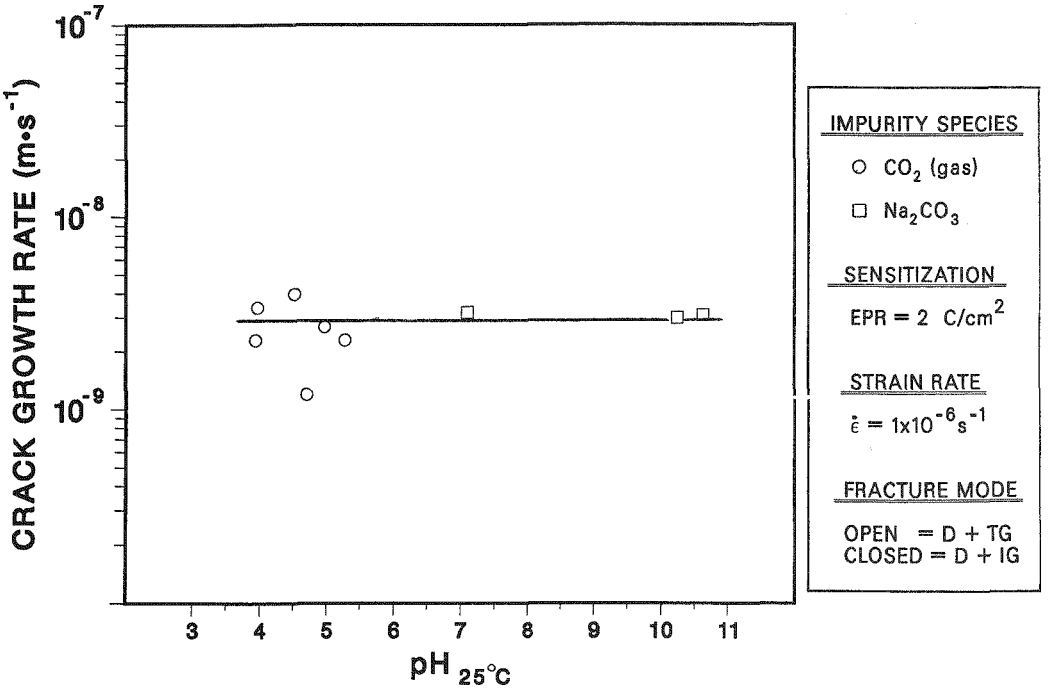

(c)

Figure 16. contd.

values as a function of calculated $pH_{289°C}$ in Figs. 18b and 19b are ≈100 to 200 mV above the hydrogen-evolution line (a) in the figures over the $pH_{289°C}$ range of ≈4.8 to 8.0. The ECP values in the CERT tests in low-oxygen water containing carbonate are considerably below the "critical potential" for IGSCC of >–250 mV(SHE) at 289°C.[35-37] Consequently, it is not surprising that only TGSCC occurred at a relatively low rate in this series of experiments. Previous CERT results in oxygenated water (≈200 ppb) with 100 ppb CO_3^{2-} (added as acid or Na_2CO_3) indicated that carbonate had virtually no effect on intergranular crack growth rates.[38] The latter results are consistent with those of Ljungberg et al.[39]

4 Environmentally Assisted Cracking of Ferritic Steels

Plain carbon steels are used extensively in PWR and BWR nuclear steam supply systems as piping and pressure vessel materials. The steels of interest for these applications include A106-Gr B and A333-Gr 6 for seamless pipe and A302-Gr B, A508-2, and A533-Gr B plate for pressure vessels. Although operating experience with ferritic steel components in reactor pressure boundaries is much better than with weld-sensitized austenitic stainless steels, instances of cracking of these steels have occurred in plants in the U.S. and abroad.

Ferritic steels become susceptible to TGSCC in high-temperature water containing dissolved oxygen and some evidence suggests a synergistic effect between oxygen and soluble copper compounds (viz., $CuCl_2$), as well as other impurities, to produce susceptibility to SCC.

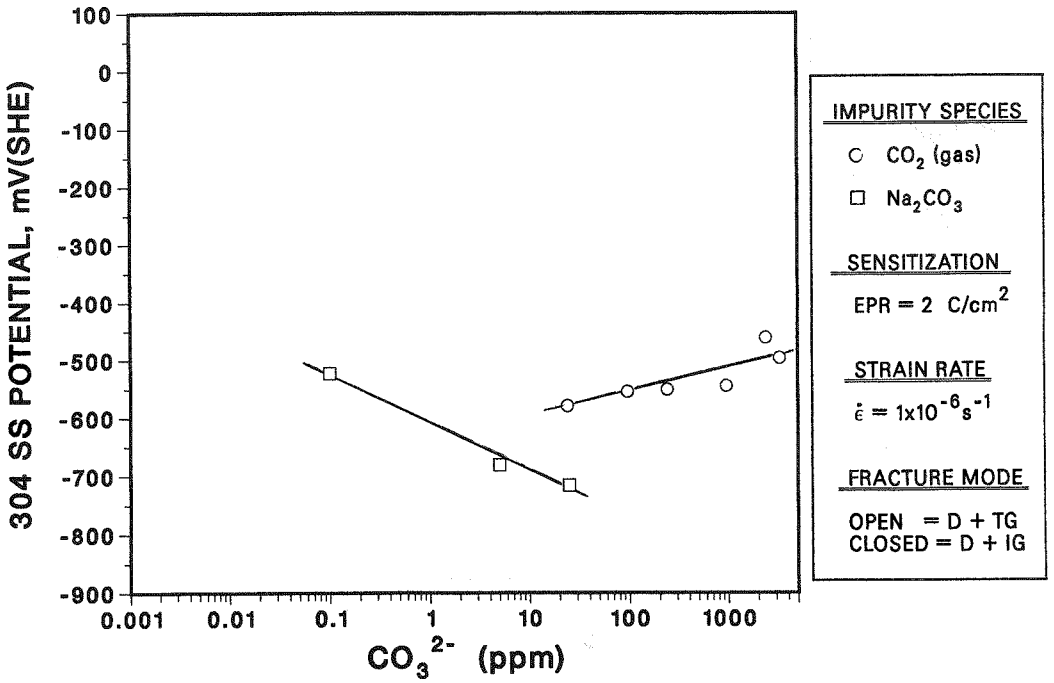

(a)

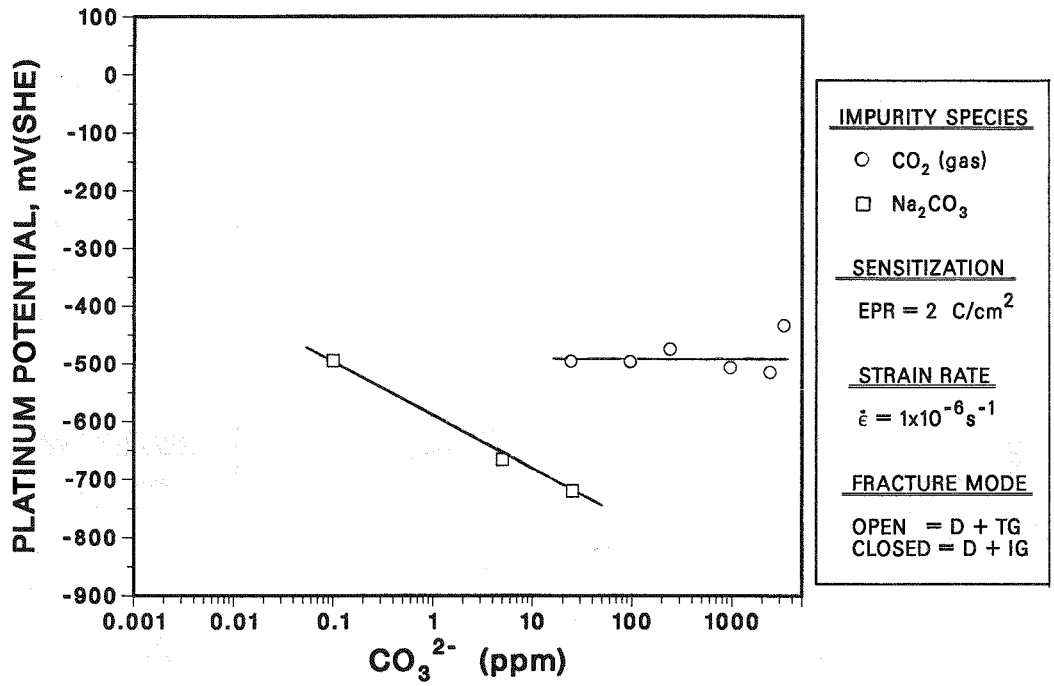

(b)

Figure 17. Dependence of the Steady-State Electrochemical Potential of (a) Type 304 SS and (b) Platinum on the Concentration of Carbonate of the Low-Oxygen (<5 ppb) Feedwater during CERTs on Sensitized Type 304 SS Specimens at 289°C.

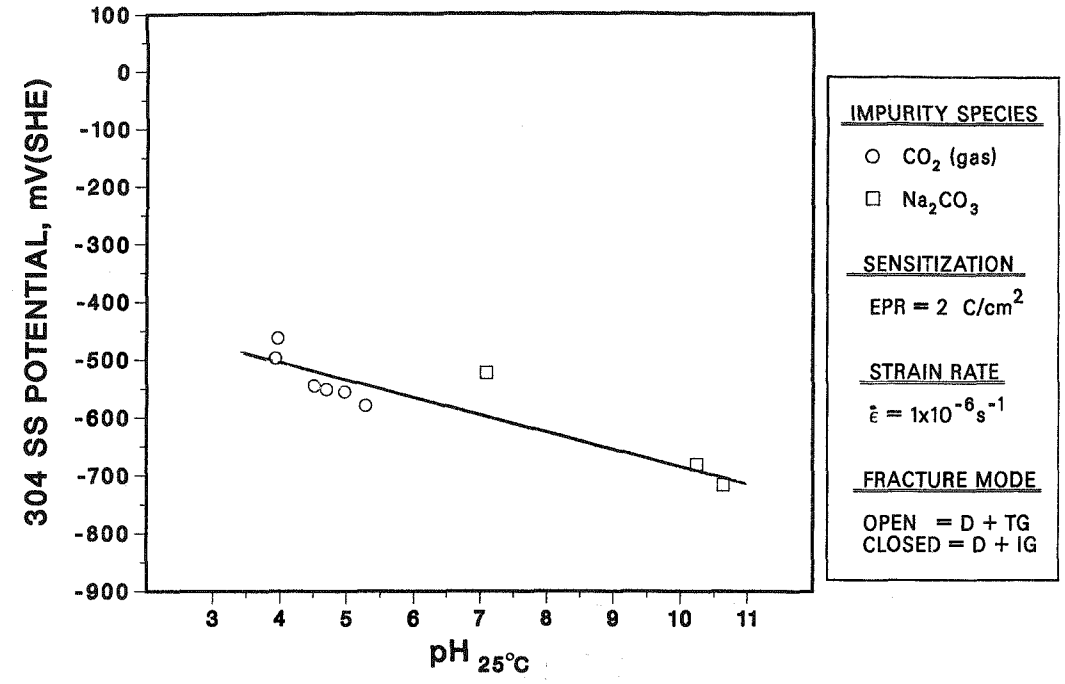

(a)

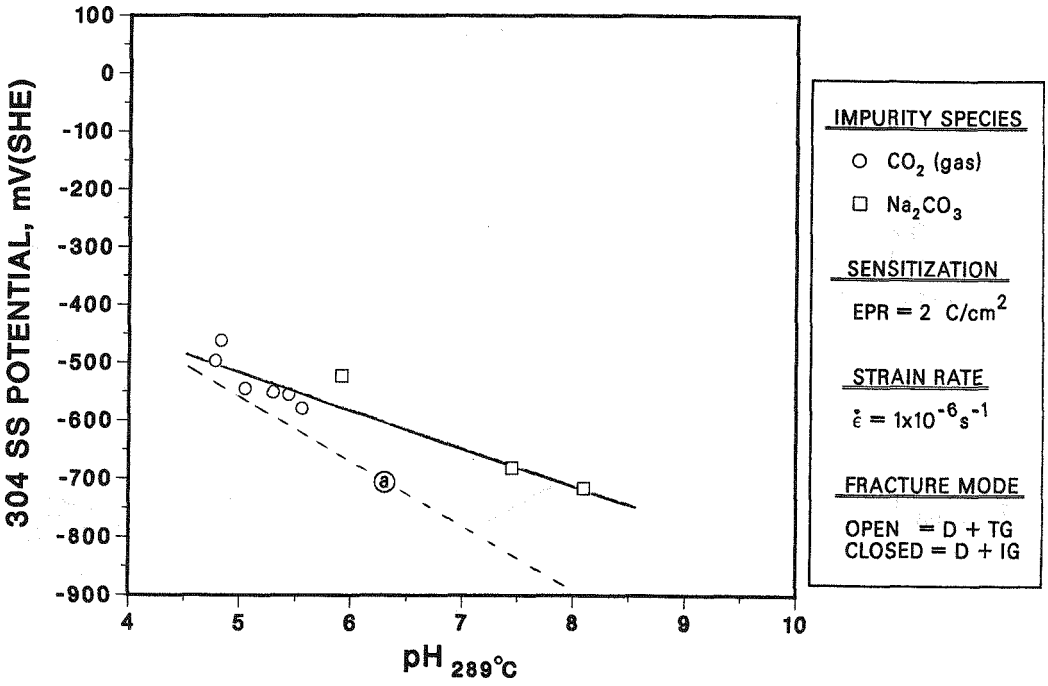

(b)

Figure 18. Dependence of the Steady-State Electrochemical Potential of Type 304 SS on (a) $pH_{25°C}$ and (b) Calculated $pH_{289°C}$ of the Low-Oxygen (<5 ppb) Feedwater during CERTs on Sensitized Type 304 SS Specimens at 289°C. Dashed line in (b) denotes the hydrogen evolution reaction.

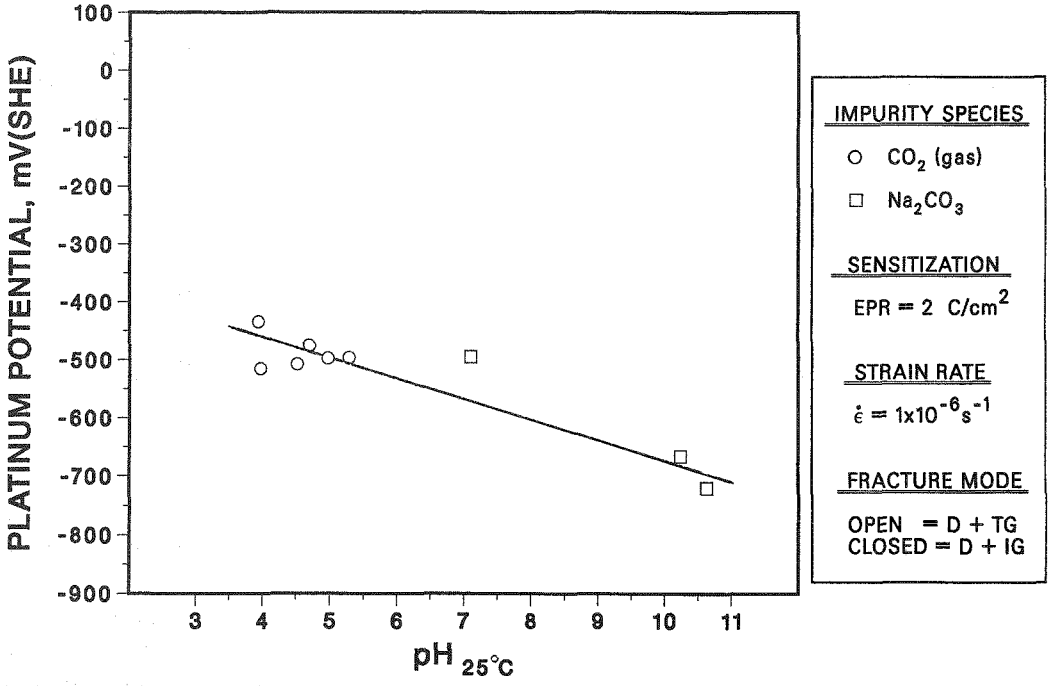

(a)

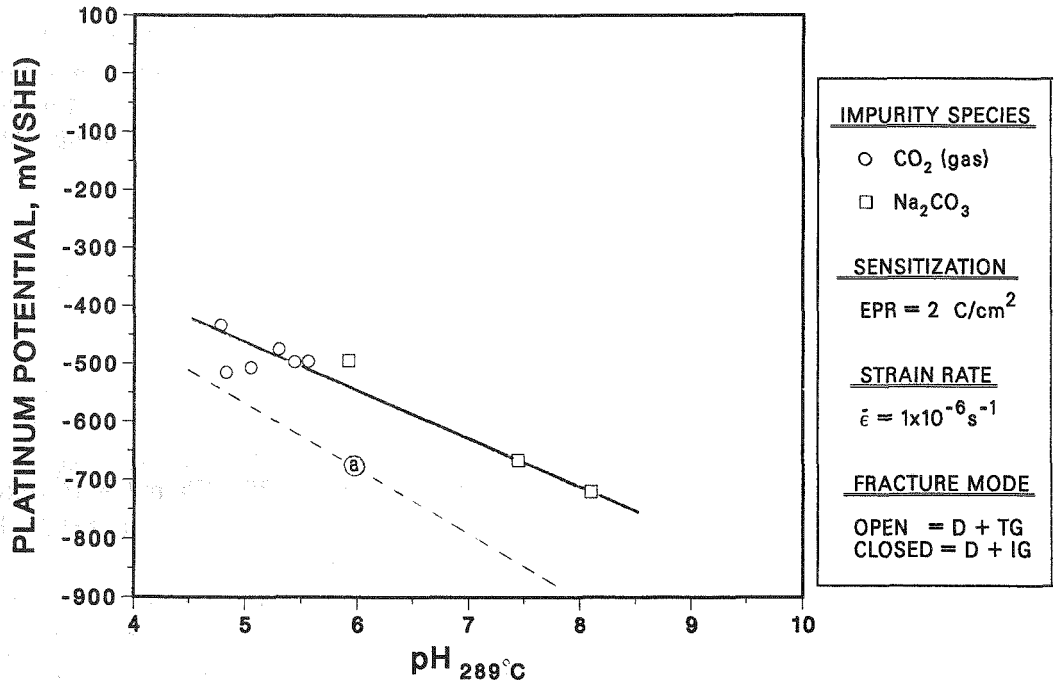

(b)

Figure 19. Dependence of the Steady-State Electrochemical Potential of Platinum on (a) $pH_{25°C}$ and (b) Calculated $pH_{289°C}$ of the Low-Oxygen (<5 ppb) Feedwater during CERTs on Sensitized Type 304 SS Specimens at 289°C. Dashed line in (b) denotes the hydrogen evolution reaction.

However, the ranges of dissolved oxygen and impurity concentrations that can lead to SCC in these materials remain relatively ill-defined. The objective of this work is to characterize the environmental and material conditions that can produce SCC susceptibility in these steels.

4.1 Technical Progress

4.1.1 Crack-Growth-Rate Tests (J. Y. Park, W. E. Ruther, and T. F. Kassner)

Fracture-mechanics CGR tests are being performed on specimens from a plate of A533-Gr B pressure vessel steel (Heat No. 02, containing 0.018% sulfur and 0.012% phosphorus) in deionized water with ≈200 ppb dissolved oxygen at 289°C.

In one test system, a composite 1TCT specimen of ferritic steel/Inconel-182/Inconel-600, which was fabricated by overlaying the ferritic steel with In-182 weld metal and then electron-beam welding In-600 to the In-182, is being tested. The specimen is designed so that the crack will proceed from the In-182 into the ferritic steel. The specimen was nickel-plated to prevent contact of the large surface of low-alloy steel with the environment in order to simulate a crack in a clad low-alloy steel vessel. In another test system a conventional 1TCT ferritic specimen, a nickel-plated specimen, and a gold-plated specimen are being tested. The plated specimens are included to determine whether electron transfer through the oxide film on the bulk surface of the ferritic steel is important in the overall SCC process, and hence, to assess the validity of using data obtained from specimens without cladding to analyze the behavior of a clad ferritic vessel, where only the crack surface is exposed to the environment. The composite specimen is intended to address the question of whether the K_{ISCC} value determined from conventional fatigue precracked specimens is applicable to the more prototypical case when a crack in the ferritic steel initiates from a stress corrosion crack in the In-182 weld metal.

The composite specimen was fatigue-precracked in the environment and the SCC test was initiated at a load ratio of 0.95, a frequency of 0.08 Hz, and a K_{max} of 28 MPa·m$^{1/2}$. Crack growth in the In-182 weld metal of the composite specimen occurred at a rate of 2.5 x 10^{-10} m·s^{-1} for the first 1800 h, i.e., a rate typical of austenitic SS under similar loading conditions. Crack length measurements indicate that the crack tip reached the interface between the In-182 weld metal and the low-alloy steel, but did not enter the ferritic material. The K_{max} value was then increased from 31 to 35 MPa·m$^{1/2}$ to determine if cracking would resume at the higher stress intensity. After one week (≈170 h), the compliance measurement indicated an increase in crack length of ≈0.4 mm, but during a subsequent four-week period no additional crack growth occurred. Because no sustained crack growth was observed at this stress intensity level, the K_{max} value was then increased to 40 MPa·m$^{1/2}$, and again no significant sustained crack growth was observed. Crack length increased ≈0.9 mm within a ≈170-h period, but during an additional ≈1100-h period, the crack advanced only ≈0.18 mm, which corresponds to a CGR of ≈5 x 10^{-11} m·s^{-1}. The K_{max} value was increased to 45 MPa·m$^{1/2}$ and no measurable crack growth occurred in an ≈840-h period. The K_{max} value has been increased to 50 MPa·m$^{1/2}$ and the tests are continuing.

In the other system, the conventional and the nickel- and gold-plated specimens were precracked under a cyclic load (a sawtooth wave shape with 12-s loading and 1-s unloading time) of R = 0.25 at 0.08 Hz and a maximum initial stress intensity of 20 MPa·m$^{1/2}$. During this precracking phase, the CGRs were 4 x 10^{-9} m·s^{-1} for the conventional and nickel-plated specimens and 2 x 10^{-8} m·s^{-1} for the gold-plated specimen, i.e., the CGR of the gold-plated specimen was higher than those of the other specimens by a factor of 5. Crack length is determined by the DC potential method; however, calibration of the measurements for the plated specimens has not been verified because the tests are still in progress.

After fatigue precracking, the load ratio was changed to R = 0.95 and the crack growth tests were continued in the same environment for ≈1700 h at a frequency of 0.08 Hz and different stress intensity values in the range of 21 to 31 MPa·m$^{1/2}$ for the conventional and nickel-plated specimens and 23 to 34 MPa·m$^{1/2}$ for the gold-plated specimen. No crack growth was observed in any of the specimens for this range of stress intensity values. To reinitiate crack growth, the load ratio was lowered to R = 0.5 for 23.5 h and fast crack growth occurred in all three specimens. Average CGRs were 5 x 10^{-8}, 6 x 10^{-8}, and 4 x 10^{-8} m·s^{-1} for the conventional, the nickel-plated, and gold-plated specimens, respectively. Because of this crack growth under R = 0.5 loading, the maximum stress intensity values increased from 31 to 38 (conventional specimen), 31 to 39 (nickel-plated specimen), and 34 to 40 MPa·m$^{1/2}$ (gold-plated specimen).

The CGR tests were then continued under R = 0.95 for 338 h, R = 0.8 for 73 h, and at R = 0.9 for 74 h. Under R = 0.95, no crack growth occurred in any of the three specimens, except for transient growth in the gold-plated specimen at a rate of 9 x 10^{-11} m·s^{-1} during the initial 150-h period. Under R = 0.8 loading, no crack growth occurred in the conventional specimen, but fast crack growth occurred in the nickel- and gold-plated specimens at average rates of 3 x 10^{-8} and 2 x 10^{-8} m·s^{-1}, respectively. Because of this crack growth under R = 0.8 loading, the maximum stress intensity values increased from 39 to 58 MPa·m$^{1/2}$ (nickel-plated specimen), and 40 to 50 MPa·m$^{1/2}$ (gold-plated specimen). The maximum stress intensity for the conventional specimen remained unchanged at 38 MPa·m$^{1/2}$. Under R = 0.9 loading, no crack growth occurred in the conventional specimen, but the nickel- and gold-plated specimens cracked at average rates of 4 x 10^{-10} and 6 x 10^{-10} m·s^{-1}, as shown in Fig. 20. These growth rates are lower by a factor of ≈50 than those at R = 0.8. Due to crack growth under R = 0.9 loading, the maximum stress intensity values increased slightly from 58 to 59 (nickel-plated specimen No. 02C-5), and 50 to 51 MPa·m$^{1/2}$ (gold-plated specimen No. 02C-6). The maximum stress intensity value for the conventional specimen (No. 02C-4) remained unchanged at 38 MPa·m$^{1/2}$. The load ratio has been increased to R = 0.95, and the tests are continuing.

5 Summary of Results

5.1 Influence of Load Ratio and Stress Intensity on CGR of Types 316NG and CF-3M SS

- Sustained crack growth occurs in Type 316NG SS only at stress intensity factors ≥22 MPa·m$^{1/2}$ under high-R (0.95) loading in 289°C oxygenated water containing 100 ppb SO_4^{2-}. The CGR decreases by a factor of ≈2 to 3 under constant load (R = 1) at the same stress intensity factor and water chemistry conditions.

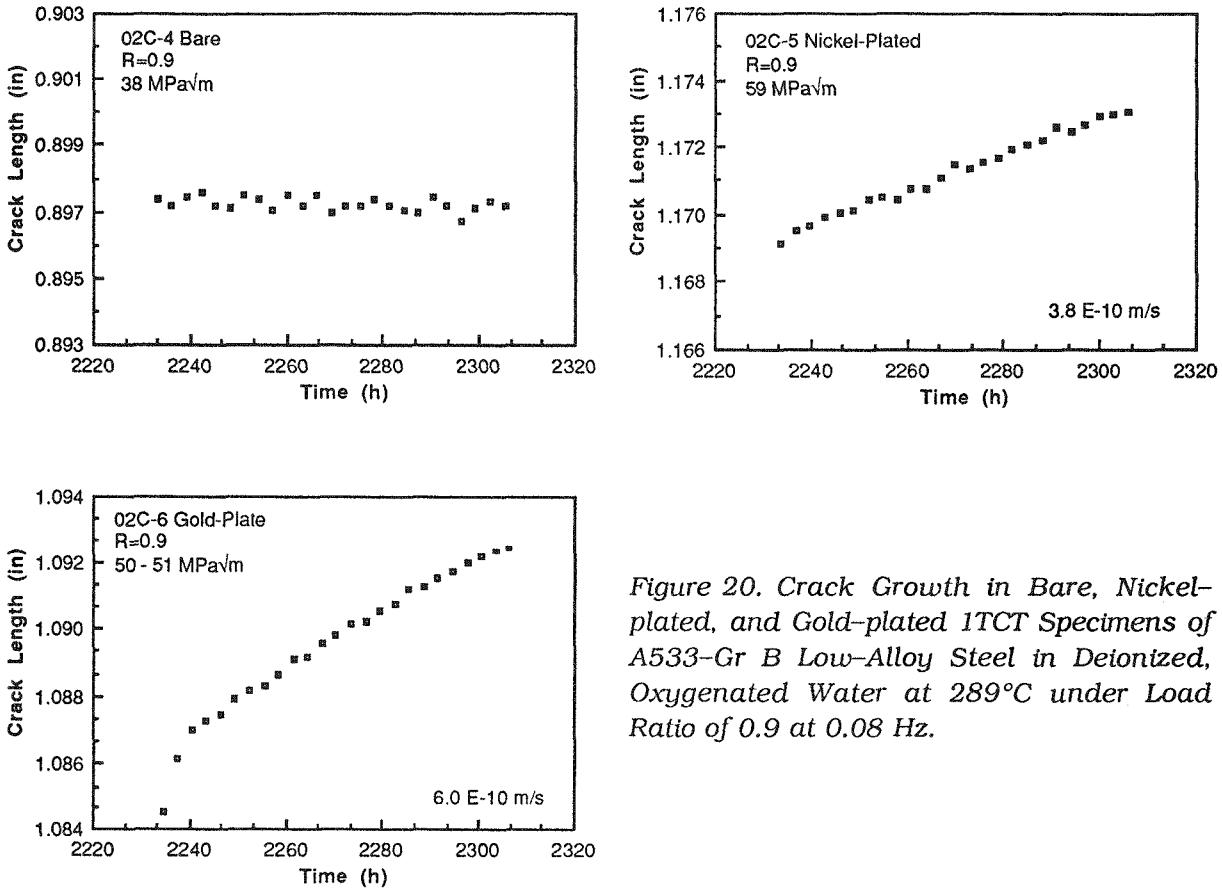

Figure 20. Crack Growth in Bare, Nickel-plated, and Gold-plated 1TCT Specimens of A533-Gr B Low-Alloy Steel in Deionized, Oxygenated Water at 289°C under Load Ratio of 0.9 at 0.08 Hz.

- A fine-grain cast CF-3M steel cracks at a slightly higher rate than Type 316NG SS under the same loading and water chemistry conditions. Cracking mode in both steels was transgranular.

5.2 Influence of Organic Acids in Oxygenated Water on CGR of Type 316NG SS

- Short-chain carboxylic acids (viz., propionic or butyric) at low concentrations (<100 ppb) in oxygenated water do not mitigate TGSCC of Type 316NG SS under high-R, low-frequency loading, in contrast to their beneficial effect on IGSCC of sensitized Type 304 SS under analogous conditions. This difference in behavior can be rationalized in terms of the differences in the repassivation characteristics of the material in the crack paths of the two steels (nonsensitized versus sensitized), as influenced or limited by the concomitant cathodic reduction of dissolved oxygen in a macrocell corrosion process.

5.3 Crack Growth Tests on Welded Type 316NG and 304 SS Pipe

- Tests on 4-in.-diameter welded pipe specimens of Types 316NG and 304 SS were conducted in simulated BWR water at Battelle Pacific Northwest Laboratory. No failures occurred during a test time of ≈8500 h in low-oxygen water containing ≈100 ppb SO_4^{2-}. In water with ≈200 ppb dissolved oxygen and ≈100 ppb SO_4^{2-}, conventional Type 304

SS welds developed through-wall cracks after ≈700 cycles. Welds of Type 316NG SS have accumulated >10 times as many cycles without failure.

5.4 Fatigue of Type 316NG SS in Simulated BWR Water

- Fatigue tests on Type 316NG SS are being performed in 288°C oxygenated water to assess the degree of conservatism inherent in the ASME Code Section III Fatigue design curves. The normalized fatigue life N_{env}/N_{air} depends primarily on strain rate and is relatively independent of strain range. At the lowest strain rates in the tests, the fatigue life in water is about one-third of that in air.

5.5 Water Chemistry Influence on SCC of Type 304 SS

- The effect of carbonate ion at concentrations between ≈0.1 and 3300 ppm in low-oxygen water (<5 ppb) on SCC of sensitized Type 304 SS was investigated in CERT tests at 289°C. Only TGSCC occurred at a relatively low rate (≈3 x 10^{-9} m·s^{-1}) that was independent of carbonate concentration and pH of the water.

- Carbonate is the only oxyanion species that is capable of cathodic reduction (to formate) in which the CGRs have not exhibited a dependence on the anion concentration raised to a simple power (e.g., 1/2). This, in part, can be attributed to the electrochemical potential of the steel, which was below the critical potential of ≈–250 mV(SHE) for IGSCC in all of the experiments.

5.6 SCC of Ferritic Steels

- Fracture-mechanics CGR tests are being performed on an A533-Gr B steel specimen and a composite specimen that was fabricated by overlaying the ferritic steel with In-182 weld metal. While crack growth occurred at a rate of ≈2.5 x 10^{-10} m·s^{-1} in the In-182 weld metal at stress intensity values of <30 MPa·m$^{1/2}$, sustained cracking has not occurred in the underlying ferritic steel at stress intensity values up to 50 MPa·m$^{1/2}$.

- Initial CGR tests on nonplated (conventional) and nickel- and gold-plated low-alloy steel specimens under high-R loading in the same autoclave indicate that the plated specimens, which simulate a crack in clad low-alloy steel vessel, exhibit higher crack growth rates than the conventional specimen.

References

1. W. E. Ruther, W. K. Soppet, and T. F. Kassner, in *Environmentally Assisted Cracking in Light Water Reactors: Semiannual Report, October 1986–March 1987*, NUREG/CR-4667 Vol. IV, ANL-87-41, pp. 47-53 (December 1987).

2. W. E. Ruther, W. K. Soppet, and T. F. Kassner, in *Environmentally Assisted Cracking in Light Water Reactors: Semiannual Report, April–September 1987*, NUREG/CR-4667 Vol. V, ANL-88-32, pp. 28-38 (February 1989).

3. W. E. Ruther, W. K. Soppet, J. Y. Park, and T. F. Kassner, in *Environmentally Assisted Cracking in Light Water Reactors: Semiannual Report, October 1987–March 1988*, NUREG/CR–4667 Vol. 6, ANL–89/10, pp. 5–12 (August 1989).

4. W. E. Ruther, W. K. Soppet, and T. F. Kassner, in *Environmentally Assisted Cracking in Light Water Reactors: Semiannual Report, April–September 1988*, NUREG/CR–4667 Vol. 7, ANL–89/40, pp. 29–37 (February 1990).

5. W. E. Ruther, W. K. Soppet, and T. F. Kassner, in *Light–Water–Reactor Safety Research Programs: Quarterly Progress Report, January–March 1985*, NUREG/CR–4490 Vol. I, ANL–85–75 Vol. I (March 1986), pp. 25–42.

6. P. S. Maiya and W. J. Shack, in *Light–Water–Reactor Safety Research Programs: Quarterly Progress Report, October–December 1984*, NUREG/CR–3998 Vol. III, ANL–84–60 Vol. III, pp. 14–23 (October 1985).

7. P. S. Maiya, *J. of Press. Ves. Technol.* **109**, 116–123 (1987).

8. J. C. Huang, R. K. Sen, and E. Yeager, *J. Electrochem. Soc.* **126**, 786–792 (1979).

9. S. M. Kaska, S. Sarangapani, and Jose Giner, *J. Electrochem. Soc.* **136**, 79–83 (1989).

10. W. E. Ruther, W. K. Soppet, and T. F. Kassner, in *Materials Science and Technology Division Light–Water–Reactor Safety Research Program: Quarterly Progress Report, October–December 1983*, NUREG/CR–3689 Vol. IV, ANL–83–85 Vol. IV, pp. 75–87 (August 1984).

11. W. E. Ruther, W. K. Soppet, and T. F. Kassner, in *Light–Water–Reactor Safety Research Programs: Quarterly Progress Report, January–March 1985*, NUREG/CR–4490 Vol. I, ANL–85–75 Vol. I, pp. 43–49 (March 1986).

12. W. E. Ruther, W. K. Soppet, J. Y. Park, and T. F. Kassner, in *Environmentally Assisted Cracking in Light Water Reactors: Semiannual Report, October 1986–March 1987*, NUREG/CR–4667 Vol. IV, ANL–87–41, pp. 2–10 (December 1987).

13. W. E. Ruther, W. J. Shack, T. F. Kassner, and W. K. Soppet, in *Environmentally Assisted Cracking in Light Water Reactors: Semiannual Report, April–September 1988*, NUREG/CR–4667 Vol. 7, ANL–89/40, pp. 3–14 (February 1990).

14. F. P. Ford, "Stress Corrosion Cracking," in *Corrosion Processes*, R. N. Parkins, ed., Applied Science Publishers, New York, (1982), pp. 271–309.

15. D. A. Vermilyea, in *Proc. Intl. Conf. on Stress Corrosion Cracking and Hydrogen Embrittlement of Iron Base Alloys*, R. W. Staehle, J. Hochmann, R. D. McCright, and J. E. Slater, eds., NACE, Houston (1983), p. 208.

16. J. R. Rice and G. F. Rosengren, *J. Mech. Phys. Solids*, **16**, 1–12 (1968).

17. S. M. Bruemmer, L. A. Charlot, and B. W. Arey, *Corrosion* **44**, 328–333 (1988).

18. W. E. Ruther, W. K. Soppet, G. Ayrault, and T. F. Kassner, *Corrosion* **40**, 518–527 (1984).

19. J. G. Hines, *Corros. Sci.* **1**, 21–48 (1961).

20. P. Doig and P. E. J. Flewitt, "An Electrochemical Model for Intergranular Stress Corrosion cracking in Iron–Nickel Alloys," in *Mechanisms of Environment Sensitive Cracking of Materials*, P. R. Swann, F. P. Ford, and A. C. R. Westwood, eds., The Metals Society, London, (1977), p.113.

21. P. Doig and P. E. J. Flewitt, *Metall. Trans. A*, **12A**, 923–931 (1981).

22. H. D. Solomon, *Corrosion* **40**, 493–506 (1984).

23. W. E. Ruther, W. K. Soppet, and T. F. Kassner, in *Materials Science and Technology Division Light-Water-Reactor Safety Research Program: Quarterly Progress Report, October–December 1983*, NUREG/CR-3689 Vol. IV, ANL–83–85 Vol. IV, pp. 51–65 (August 1984).

24. A. J. Gianuzzi, "Studies on AISI Type 304 Stainless Steel Piping Weldments for Use in BWR Application," EPRI NP–944 (December 1978).

25. R. M. Horn, "Parametric Studies for Stress Corrosion in Type 304 Stainless Steel Pipe," EPRI NP–34511 (January 1984).

26. W. J. Shack and W. F. Burke, in *Environmentally Assisted Cracking in Light Water Reactors: Semiannual Report, April 1988–September 1989*, NUREG/CR–4667 Vol. 7, ANL–89/40, pp. 15–17 (March 1990).

27. B. H. Dillman, R. A. Reed, and C. C. Lin, "BWR Coolant Impurity Identification Study, Final Report," EPRI NP–4156 (August 1985).

28. B. H. Dillman, J. C. Elliot, R. A. Head, J. E. Osterle, and R. S. Tunder, "Monitoring of Chemical Contaminants in BWRs," Final Report, EPRI NP–4134 (July 1985).

29. J. E. Richards and W. A. Byers, "Industry-wide Survey of PWR Organics, Final Report," EPRI NP–4698 (July 1986).

30. W. E. Ruther, W. K. Soppet, and T. F. Kassner, in *Environmentally Assisted Cracking in Light Water Reactors: Semiannual Report, April–September 1985*, NUREG/CR–4667 Vol. I, ANL–86–31, pp. 27–41 (June 1986).

31. W. E. Ruther, W. K. Soppet, and T. F. Kassner, in *Environmentally Assisted Cracking in Light Water Reactors: Semiannual Report, April–September 1988*, NUREG/CR–4667 Vol. 7, ANL–89/40, pp. 17–29 (February 1990).

32. W. E. Ruther, W. K. Soppet, and T. F. Kassner, in *Environmentally Assisted Cracking in Light Water Reactors: Semiannual Report, October 1986–March 1987*, NUREG/CR-4667 Vol. IV, ANL-87-41, pp. 35–47 (December 1987).

33. W. E. Ruther, W. K. Soppet, and T. F. Kassner, in *Environmentally Assisted Cracking in Light Water Reactors: Semiannual Report, April–September 1987*, NUREG/CR-4667 Vol. V, ANL-88-32, pp. 24–37 (February 1989).

34. W. E. Ruther, W. K. Soppet, and T. F. Kassner, in *Environmentally Assisted Cracking in Light Water Reactors: Semiannual Report, October 1987–March 1988*, NUREG/CR-4667 Vol. 6, ANL-89/10, pp. 27–42 (August 1989).

35. J. N. Kass and R. L. Cowan, "Hydrogen Water Chemistry for BWRs," in *Environmental Degradation of Materials in Nuclear Power Systems–Water Reactors, Proc. of the 2nd Int. Symp.*, Monterey, CA, September 9–12, 1985, ANS, La Grange Park, IL (1986), pp. 211–218.

36. M. E. Indig, B. M. Gordon, R. B. Davis, and J. E. Weber, "Evaluation of In-reactor Stress Corrosion Cracking via Electrochemical Measurements," ibid., pp. 411–418.

37. D. D. Macdonald and G. Cragnolino, "The Critical Potential for IGSCC of Sensitized Type 304 SS in High Temperature Aqueous Systems," ibid., pp. 426–434.

38. W. E. Ruther, W. K. Soppet, and T. F. Kassner, *Corrosion* **44**, 791–799 (1988).

39. L. G. Ljungberg, D. Cubicciotti, and M. Trolle, "Effects of Water Impurities on Environmental Cracking in BWRs," in *Environmental Degradation of Materials in Nuclear Power Systems–Water Reactors, Proc. of the 2nd Int. Symp.*, Monterey, CA, September 9–12, 1985, ANS, La Grange Park, IL (1986), pp. 435–441.

Distribution for NUREG/CR-4667 Vol. 8 (ANL-90/4)

Internal:

W. J. Shack (30)

TIS File (3)

ANL Patent File

ANL Contract File

External:

NRC, for distribution per R5 (315)

ANL Libraries (2)

Manager, Chicago Operations Office, DOE

Materials and Components Technology Division Review Committee:

- P. A. Alexander, Lord Corp., Erie, PA
- M. S. Dresselhaus, Massachusetts Institute of Technology, Cambridge, MA
- S. J. Green, Electric Power Research Institute, Palo Alto, CA
- R. A. Greenkorn, Purdue University, West Lafayette, IN
- L. J. Jardine, Lawrence Livermore National Laboratory, CA
- C.-Y. Li, Cornell University, Ithaca, NY
- R. E. Scholl, Counter Quake Corp., Redwood City, CA
- P. G. Shewmon, Ohio State University, Columbus, OH
- R. Smith, EPRI NDE Center, Charlotte, NC

P. L. Andresen, General Electric Corporate Research and Development, Schenectady, NY

W. H. Bamford, Structural Materials Engineering, Westinghouse Electric Corp., Pittsburgh, PA

J. A. Bonucci, Commonwealth Edison Co., Chicago, IL

R. M. Crawford, Fluor-Daniel Corp., Chicago, IL

D. Cubicciotti, Electric Power Research Inst., Palo Alto, CA

G. Cragnolino, Center for Nuclear Waste Regulatory Analysis, San Antonio, TX

W. H. Cullen, Materials Engineering Assoc., Inc., Lanham, MD

J. C. Danko, U. Tennessee, Knoxville, TN

R. Duncan, Combustion Engineering, Inc., Windsor, CT

M. Fox, APTECH, Sunnyvale, CA

Y. S. Garud, S. Levy, Inc., Campbell, CA

F. Garzarolli, KWU, Erlangen, West Germany

B. M. Gordon, General Electric Co., San Jose, CA

S. D. Harkness, Bettis Atomic Power Laboratory, West Mifflin, PA

D. Harrison, USDOE, Germantown, MD

M. E. Indig, General Electric Co., Pleasanton, CA

NRC FORM 335 (2–89) NRCM 1102, 3201, 3202

U. S. NUCLEAR REGULATORY COMMISSION

BIBLIOGRAPHIC DATA SHEET

(See instructions on the reverse)

1. REPORT NUMBER *(Assigned by NRC. Add Vol., Supp., Rev., and Addendum Numbers, if any.)*
NUREG/CR–4667 Vol. 8
ANL–90/4

2. TITLE AND SUBTITLE
Environmentally Assisted Cracking in Light Water Reactors
Semiannual Report October 1988—March 1989

3. DATE REPORT PUBLISHED
MONTH: June
YEAR: 1990

4. FIN OR GRANT NUMBER
A2212

5. AUTHOR(S)
T. F. Kassner, J. Y. Park, W. E. Ruther,
W. J. Shack, D. R. Diercks, and W. K. Soppet

6. TYPE OF REPORT
Technical; Semiannual

7. PERIOD COVERED *(Inclusive Dates)*
10/88–3/89

8. PERFORMING ORGANIZATION – NAME AND ADDRESS *(If NRC, provide Division, Office or Region, U.S. Nuclear Regulatory Commission, and mailing address; if contractor, provide name and mailing address.)*

Argonne National Laboratory
9700 South Cass Avenue
Argonne, IL 60439

9. SPONSORING ORGANIZATION – NAME AND ADDRESS *(If NRC, type "Same as above": if contractor, provide NRC Division, Office or Region, U.S. Nuclear Regulatory Commission, and mailing address.)*

Division of Engineering
Office of Nuclear Regulatory Research
U. S. Nuclear Regulatory Commission
Washington, DC 20555

10. SUPPLEMENTARY NOTES

11. ABSTRACT (200 words or less)

This report summarizes work performed by Argonne National Laboratory on environmentally assisted cracking in light water reactors during the six months from October 1988 to March 1989. The effects of load ratio on stress corrosion cracking (SCC) of Types 316NG, 304, and CF–3M cast stainless steels (SSs) were investigated by fracture–mechanics crack–growth–rate (CGR) tests in high–temperature water. The influence of organic impurities on the SCC of Type 316NG SS was also investigated in long–term CGR tests. Tests to determine the susceptibility of 4–in.–diameter Types 316NG and 304 SS pipe weldments to SCC in simulated BWR environments have been conducted. The influence of carbonate at concentrations between 0.1 and 3300 ppm on the SCC behavior of sensitized Type 304 SS in deoxygenated water (<5 ppb) was determined in constant–extension–rate–tensile (CERT) tests. Fatigue tests were conducted on Type 316NG SS in air and BWR environments to assess the degree of conservatism in the ASME Code Section III fatigue design curves. CGR tests to determine susceptibility to SCC are being conducted on A533–Gr B low–alloy ferritic steel in simulated BWR environments.

12. KEY WORDS/DESCRIPTORS *(List words or phrases that will assist researchers in locating this report.)*

Water Chemistry
Corrosion
Stress Corrosion Cracking
Crack Growth

13. AVAILABILITY STATEMENT
Unlimited

14. SECURITY CLASSIFICATION
(This Page)
Unclassified
(This Report)
Unclassified

15. NUMBER OF PAGES

16. PRICE

H. S. Isaacs, Brookhaven National Laboratory, Upton, NY

R. H. Jones, Battelle Pacific Northwest Laboratory, Richland, WA

J. N. Kass, Lawrence Livermore National Laboratory, Livermore, CA

L. Ljungberg, ASEA-ATOM, Vasteras, Sweden

C. D. Lundin, U. Tennessee, Knoxville, TN

D. D. Macdonald, SRI International, Menlo Park, CA

H. Metha, General Electric Co., San Jose, CA

D. Morgan, Pennsylvania Power and Light Co., Allentown, PA

R. A. Oriani, U. Minnesota, Minneapolis, MN

S. Ranganath, General Electric Co., San Jose, CA

P. M. Scott, Framatom, Paris, France.

S. Smialowska, Ohio State U., Columbus, OH

D. M. Stevens, Lynchburg Research Center, Babcock & Wilcox Co., Lynchburg, VA

W. A. Van Der Sluys, Research & Development Division, Babcock & Wilcox Co., Alliance, OH

E. Venerus, Knolls Atomic Power Laboratory, Schenectady, NY

J. R. Weeks, Brookhaven National Laboratory, Upton, NY

D. Winkel, Teleco Oil Field Services, Meriden, CT

A. W. Zeuthen, Long Island Lighting Co., Wading River, NY